CHEMICAL REVIEWS

pubs.acs.org/CR Review

Electrolyte Lifetime in Aqueous Organic Redox Flow Batteries: A Critical Review

David G. Kwabi, Yunlong Ji, and Michael J. Aziz*

Cite This: *Chem. Rev.* 2020, 120, 6467−6489 Read Online

ABSTRACT: Aqueous organic redox flow batteries (RFBs) could enable widespread integration of renewable energy, but only if costs are sufficiently low. Because the levelized cost of storage for an RFB is a function of electrolyte lifetime, understanding and improving the chemical stability of active reactants in RFBs is a critical research challenge. We review known or hypothesized molecular decomposition mechanisms for all five classes of aqueous redox-active organics and organometallics for which cycling lifetime results have been reported: quinones, viologens, aza-aromatics, iron coordination complexes, and nitroxide radicals. We collect, analyze, and compare capacity fade rates from all aqueous organic electrolytes that have been utilized in the capacity-limiting side of flow or hybrid flow/nonflow cells, noting also their redox potentials and demonstrated concentrations of transferrable electrons. We categorize capacity fade rates as being "high" (>1%/day), "moderate" (0.1−1%/day), "low" (0.02−0.1%/day), and "extremely low" (≤0.02%/day) and discuss the degree to which the fade rates have been linked to decomposition mechanisms. Capacity fade is observed to be time-denominated rather than cycle-denominated, with a temporal rate that can depend on molecular concentrations and electrolyte state of charge through, e.g., bimolecular decomposition mechanisms. We then review measurement methods for capacity fade rate and find that simple galvanostatic charge−discharge cycling is inadequate for assessing capacity fade when fade rates are low or extremely low and recommend refining methods to include potential holds for accurately assessing molecular lifetimes under such circumstances. We consider separately symmetric cell cycling results, the interpretation of which is simplified by the absence of a different counter-electrolyte. We point out the chemistries with low or extremely low established fade rates that also exhibit open circuit potentials of 1.0 V or higher and transferrable electron concentrations of 1.0 M or higher, which are promising performance characteristics for RFB commercialization. We point out important directions for future research.

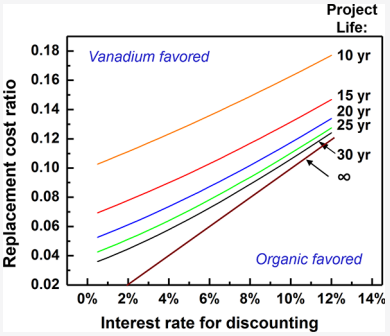

CONTENTS

1. INTRODUCTION

1.1. Flow Batteries and Storage of Renewable Energy

Increasing global energy needs, coupled with the harmful effects of CO_2 emissions on the climate, have spurred interest in the development of carbon-free energy sources.[1−3] The inherently intermittent availability of solar and wind power, however, makes their deep penetration into the energy economy, and particularly into the electricity grid, difficult. This problem can be solved by efficient, inexpensive and scalable electrical energy storage (EES) options.[4,5] Whereas several storage options such as capacitors, flywheels, and enclosed batteries exist for short-

Special Issue: Beyond Li-Ion Battery Chemistry

Received: September 22, 2019
Published: February 13, 2020

https://dx.doi.org/10.1021/acs.chemrev.9b00599
Chem. Rev. 2020, 120, 6467−6489

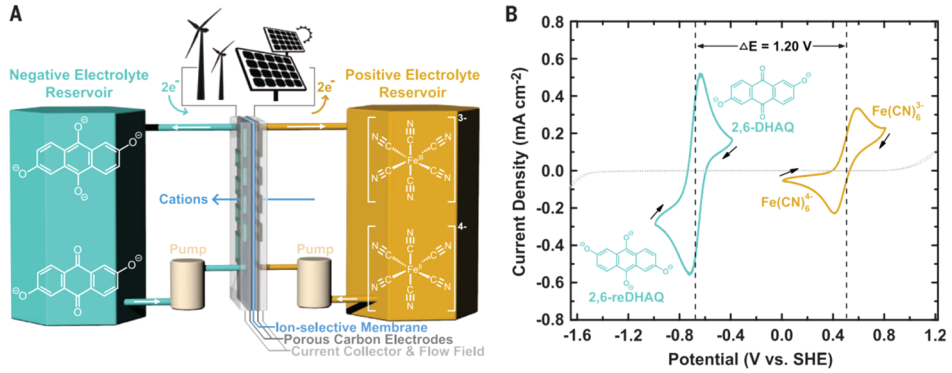

Figure 1. (a) Schematic of an RFB during battery charging. (b) Cyclic voltammogram curves showing redox reactions involving 2,6-dihydroxyanthraquinone in the negolyte and ferricyanide in the posolyte, with vertical dotted lines indicating associated reduction potentials. The dotted baseline represents the background cyclic voltammogram of a graphite foil electrode in 1 M KOH. Reprinted with permission from ref 11. Copyright 2015 The American Association for the Advancement of Science.

duration grid services such as grid power quality and frequency regulation, the main option for storage with the long-duration discharge needed to regulate wind or solar sources is pumped hydroelectric energy storage. Pumped hydroelectric storage, however, has a large areal footprint and is geographically limited by requiring two large reservoirs at significantly different elevations. Compressed air energy storage in underground caverns requires natural gas combustion during discharge; compressed air implemented adiabatically aboveground would not require combustion but is in its infancy.

Given its lack of geographic constraints, EES in the form of secondary (i.e., rechargeable) batteries can potentially enable the storage of intermittent renewable energy at scale. Moreover, the large variety of chemistries and electrode architectures in which it can be embodied translates to a wide range of specific energy and power capabilities in secondary batteries. Despite this high operational flexibility, the only electrochemical EES system that has attracted extensive commercial attention is the rechargeable lithium-ion battery (LIB), which has facilitated the adoption of portable electronic devices in daily life. Considerable research and industrial effort has also been directed toward the incorporation of LIBs into electric vehicles. However, the prospects for their integration into long-duration grid scale storage are challenged by projected issues with scarcity, geopolitical concentration of their raw materials,[6] and fire hazards[7,8] from the organic solvents they contain.

Aqueous redox flow batteries (RFBs) are a potentially safe and cost-effective technology for grid scale storage. In an RFB, chemical energy is stored in the form of two redox-active species of disparate reduction potentials, which are dissolved or suspended in an electrolyte; the electrolyte containing the species with the lower reduction potential is referred to as the negative electrolyte ("negolyte") whereas the other electrolyte is the positive electrolyte ("posolyte"). Interconversion between stored chemical and electrical energy during battery charging or discharging is facilitated by pumping the electrolytes through an electrochemical cell (Figure 1a) where electron transfer reactions take place at a pair of porous electrodes, typically carbon-based, separated by a separator that is often an ion-selective membrane. With this design, energy storage capacity scales with the volume of the electrolyte reservoirs, concentrations of redox-active species therein, and the difference in reduction potentials of the energy-storing species (Figure 1b); whereas the power scales primarily with the active area in the electrochemical cell stack. This enables energy and power to be scaled independently, unlike in an enclosed battery. Consequently, at large energy-to-power ratios (i.e., long discharge durations at rated power), the system cost per kWh of stored energy is largely dependent on the cost of the electrolytes, rather than the cost of the electrochemical cell.[9] Although the energy density (energy stored per unit volume) and specific energy (energy stored per unit mass) of aqueous electrolytes are an order of magnitude lower than for LIBs, these metrics are of secondary importance for stationary storage. Techno-economic analysis estimates that an aqueous RFB with an open-circuit voltage of 1.5 V, total electrolyte cost of $5 per kg of active material and 150 g per mole of transferrable electrons should cost about $120/kWh at the system level, with room for further cost reductions with cheaper electrolytes and large enough production volumes.[10]

1.2. Levelized Cost and Calendar Lifetime

Minimizing electrolyte cost is critically important to enabling commercialization of RFBs. Chemistries based on vanadium in highly acidic electrolytes have attracted the most research and industrial attention,[12−14] featuring the following negolyte and posolyte redox reactions and associated reduction potentials (E^0) versus the standard hydrogen electrode (SHE):

$$V^{3+} + e^- \leftrightarrow V^{2+} \quad (E^0 = -0.255V)$$

$$VO_2^+ + 2H^+ + e^- \leftrightarrow VO^{2+} + H_2O \quad (E^0 = 0.991V)$$

respectively. The difference between these reduction potentials yields a full-cell voltage of 1.25 V for a proton concentration of 1 M, which increases with decreasing pH because only the second reaction is proton-coupled and thus has a higher potential at lower pH. Considerable strides have been made toward the development and commercialization of all-vanadium RFBs, with the largest installation, rated at 200 MW/800 MWh, currently under construction by Rongke Power in Dalian, China. However, although redox-active vanadium species are stable indefinitely, the price of vanadium is too volatile and too high on average for globally ubiquitous deployment in large-scale RFB installations. To wit, the United States' Department of Energy estimates that energy storage systems for utility-scale delivery of electricity should cost not more than $150/kWh in order to be commercially feasible,[15] and vanadium RFBs are expected to have higher system costs.[16]

As a result, inorganic RFB chemistries based on more Earth-abundant raw materials, are being developed, including

https://dx.doi.org/10.1021/acs.chemrev.9b00599
Chem. Rev. 2020, 120, 6467−6489

hydrogen−bromine,[17,18] metal-hydride,[19] sulfur−oxygen,[9] and slurry-based all-iron[20−22] configurations. Despite the generally low projected chemical costs of these systems, all of them face critical technical challenges that currently prevent them from replacing vanadium RFBs. For instance, the all-iron and sulfur−oxygen chemistries have projected chemical costs of ~6.5[9] and 1 $/kWh,[9] respectively. However, for the all-iron slurry system, spatially inhomogeneous plating of elemental iron in the negolyte may result in low capacity utilization, and the high viscosity of the slurry exacerbates mass transport and pumping losses; the sulfur−oxygen chemistry faces low power densities (<10 mW/cm^2) due to high membrane resistances and the sluggish kinetics of the oxygen reduction and evolution reactions. Hybrid zinc-based flow/nonflow configurations such as zinc-halide (zinc-bromide[23] or zinc-iodide[24,25]), zinc−iron,[26] and zinc−cerium[27] systems have also received research attention, but lose the advantage of decoupling of energy and power because zinc electroplating capacity scales with cell area, rather than electrolyte reservoir volume.

An alternative pathway toward low-cost RFBs is the use of organic and organometallic redox-active reactants. Although they are expected to yield lower full-cell energy densities than the all-vanadium system,[28,29] the high abundance of their raw material precursors potentially enables much lower electrolyte costs than vanadium, and their thermochemical properties—chiefly solubility and reduction potential—can be tailored via chemical structure modification and functionalization within a wide parameter space. Their molecular size can also be tailored to suppress the rate of undesirable permeation through membranes and separators without debilitating increases in viscosity.[30,31] It is worth noting that aqueous RFB chemistries are generally limited by a full-cell voltage of roughly 1.5−1.8 V, given the practical potential limits for the electrolysis of water. This has the effect of limiting their expected energy densities. Nonaqueous RFBs may reach substantially higher voltages and energy densities; however, these are based on low-conductivity, flammable, and expensive solvents.

A key deficiency of most organic chemistries that have been reported is capacity fade rates exceeding 0.1%/day,[32−35] chiefly caused by the decomposition of their organic constituents, although permeation of active material through the membrane also plays a nontrivial role in many studies. Such high rates of capacity fade are utterly impractical for RFB installations with project lifetimes anticipated to be decades long. Decadal chemical lifetime is not, however, strictly necessary for commercially interesting aqueous organic RFB configurations. Rather, a more appropriate goal is to achieve sufficient stability at a reasonable levelized cost of the storage chemistry, given the possibility of periodically replacing the lost electrolyte. Levelized cost in this case refers to the present value of the initial and replacement costs amortized over the energy delivered out of storage over the lifetime of the project. In particular, if the present value of a series of future replacement costs for an organic RFB system is lower than the capital cost savings from using an organic system rather than a vanadium system, then the lower-cost organic system may be the more economically preferable option (Figure 2).[36]

This trade-off is expressed quantitatively by the replacement cost ratio, defined as

$$\text{replacement cost ratio} \equiv \frac{\text{annual replacement cost}}{\text{upfront capital cost savings}}$$

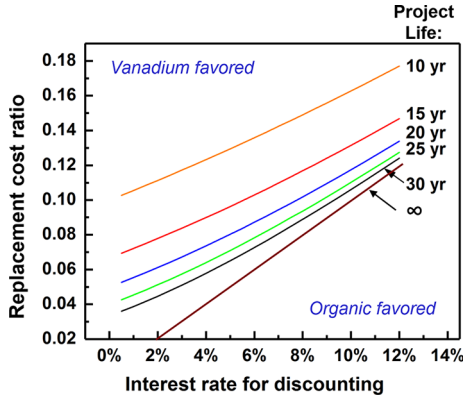

Figure 2. Breakeven value of replacement cost ratio vs interest rate for discounting, assuming project lifetimes as indicated. Adapted with permission from ref 36. Copyright 2017 John Wiley and Sons.

Because the annual replacement cost is inversely proportional to the calendar lifetime and thereby plays such a major role in this techno-economic reasoning, comprehensively understanding and mitigating temporal capacity fade in aqueous organic RFB research is a compelling and urgent research task. This review is dedicated to the status of our understanding in this respect. We particularly emphasize the importance of judicious choice of experimental method in rationalizing capacity fade in terms of specific reactant decay or loss mechanisms, as well as the temporal capacity fade rate as a more useful indicator of RFB chemical lifetime than the more often reported cycle-denominated fade rate. In addition to reactant decay, reactant permeation through the ion-selective membrane may also cause capacity loss,[37] and where appropriate, we discuss the importance of distinguishing between the two pathways for particular chemistries. We note, however, that decomposition in aqueous organic flow cells is typically the more dominant capacity fade mechanism, and that crossover should become considerable for chemistries exhibiting extremely low fade rates or inorganic redox-active species.[38−40] Other aspects of aqueous organic RFB performance, as well as issues related to aqueous metal-ion-based and nonaqueous RFB reactant chemistries, are beyond the scope of the review; interested readers are directed to surveys of studies in those fields encompassing work published in the past decade.[16,29,41−47]

2. CHEMICAL DECOMPOSITION AND CAPACITY FADE

2.1. Active Reactant Decomposition: Expectations from Theory and Chemical Studies

The chemical decomposition of organic molecules is a wide and expansive topic, however, we restrict the present discussion to the set of redox-active reactants currently under investigation in aqueous organic RFB research, which we group here into the following classes: (i) quinones, (ii) organometallic coordination complexes, (iii) nitroxide radical derivatives, (iv) viologens, and (v) all other aromatic heterocycles. Thus, in this review, we consider only those mechanisms to which species from these classes have been hypothesized or shown to be susceptible, which would lead to loss or diminution of redox activity, such as (Scheme 1): (i) nucleophilic addition or substitution such as gem-diol formation, Michael addition and hydrolysis, (ii) disproportionation to redox-inactive centers, (iii) dimerization or polymerization, and (iv) tautomerization.

https://dx.doi.org/10.1021/acs.chemrev.9b00599
Chem. Rev. 2020, 120, 6467−6489

Scheme 1. Illustration of the Main Chemical Decomposition Mechanisms for Redox-Active Molecules Considered in This Review

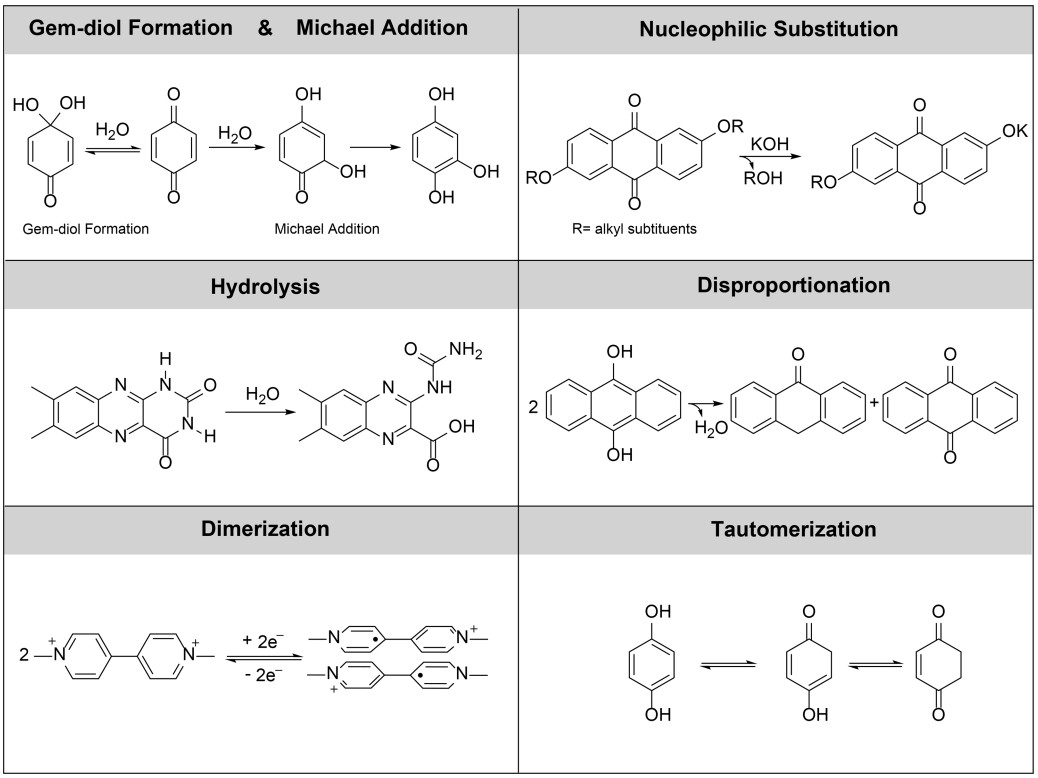

Because the number of possible combinations of RFB reactant solubility, reduction potential and decomposition mechanisms is practically infinite, rapid computational screening of large databases of particular redox-active molecule types and their thermochemical properties has attracted attention recently. With regard to quinones, Er et al. introduced a high-throughput computational screening protocol[48] to generate a virtual library of 10 000 molecules. Using density functional theory (DFT), they examined the influence of selected functional groups and their spatial positioning on the quinones' reduction potentials and solvation energies and sought to identify structure−property trends that could inform how solubility and reduction potential may be rationally tuned. Analysis of the results yielded two important conclusions: (i) at least 31 and 28 synthesizable quinones had reduction potentials below 0.2 V and above 0.9 V vs SHE, respectively, and (ii) placement of long alkyl chains with terminal hydrophilic functional groups increased quinone solubility without affecting reduction potential, whereas attaching electron-withdrawing or-donating groups close to the ketone group had a large impact on the quinone's reduction potential. This latter point was buttressed by recent combined experimental-DFT studies by Huynh et al.[49] and Kim et al.[50,51] In the report by Huynh, it was found that a quinone's reduction potential scales linearly with its attached substituents' effective Hammett constant, which is an estimate of the substituents' electron-withdrawing ability. The study, however, noted significant deviations from the scaling relationship for quinones featuring intramolecular hydrogen bonding, as well as halogenated, charged, or sterically bulky substituents.

There has been some experimental support of these proposed relationships among functional group chemistry and positioning, and reactant reduction potential. Gerhardt et al. showed that it is possible to tune the reduction potential of an anthraquinone derivative through manipulating the number, position and hydrophilicity of the functional groups attached to it.[52] For example, anthraquinone sulfonic acid (AQS) exhibits a ∼20 mV lower reduction potential than anthraquinone disulfonic acid (AQDS), due to the removal of one of the electron-withdrawing sulfonic acid groups. Dihydroxyanthraquinone disulfonic acid (DHAQDS) in turn has an ∼80 mV lower reduction potential than AQS, owing to the installation of two electron-donating hydroxyl groups next to one of the ketone groups. Distancing the electron-withdrawing sulfonic acid groups from the redox-active center, as in dihydroxyanthraquinone dimethylsulfonic acid (DHAQDMS), lowers the reduction potential of the quinone by another ∼100 mV.

The influence of substituent hydrophilicity and location on solubility follows trends suggested by theory but is not quantitatively understood. In agreement with the study by Er et al.,[48] 4,4′-((9,10-anthraquinone-2,6-diyl)dioxy)dibutyrate (2,6-DBEAQ) has been shown to have a significantly higher solubility[53] than 2,6-dihydroxyanthraquinone (2,6-DHAQ)[11] under alkaline conditions (>1 M vs 0.6 M at pH 14; 0.6 M vs 0.1 M at pH 12), ostensibly due to the carboxylate solubilizing groups of the former being located farther away from the anthraquinone core. Replacing the carboxylate functional groups with more hydrophilic phosphonate groups in 2,6-di(3-phosphonic acid)propyl ether anthraquinone (2,6-DPPEAQ)[54] boosts the solubility even further (0.75 M vs 35 mM at pH 9). However, depending on the molecule class, other strategies for modifying reactant solubility based on other chemical principles are possible. For instance, based on computational work suggesting that asymmetric charge distribution improves organic molecule solubility,[55] Hollas et al.[34] synthesized dihydroxyphenazine sulfonate (DHPS), which has a considerably higher solubility than the parent phenazine molecule under strongly alkaline conditions (1.80 M vs near-zero at pH 14). Luo et al. have also shown that replacing the

https://dx.doi.org/10.1021/acs.chemrev.9b00599
Chem. Rev. 2020, 120, 6467−6489

cation in potassium ferrocyanide ($K_4Fe(CN)_6$) or sodium ferrocyanide with the more hydrophilic ammonium cation roughly doubles the $Fe(CN)_6^{4-}$ solubility at pH 7 from 0.76 or 0.56 M, respectively, to 1.56 M;[56] however, generally reliable quantitative structure−property relationships for organic molecule solubility do not exist.

Nucleophilic addition or substitution is one of the most common modes of chemical decomposition for aqueous RFB reactants, and a number of computational studies have examined their thermodynamic susceptibility to such attack. It occurs when a nucleophilic species (such as water, hydroxyl/hydroperoxide anions, or reduced redox-active species) reacts with an electron-deficient redox-active species, typically the oxidized form of the organic redox couple. In this reaction the attacking nucleophile may either irreversibly replace a good leaving substituent attached to the molecule[57] or attach to an unsubstituted position,[58] resulting in either loss of conjugation (and hence complete loss of redox activity) or a large decrease in reactant reduction potential and/or solubility.

Chemical principles suggest that nucleophilic attack is more likely to occur as either the Lewis basicity of the nucleophile or acidity of the substrate, increases. To assess this, Tabor et al.[59] conducted a computational study of a virtual library of 140 000 benzene, naphthalene, anthracene, phenanthrene, and tetracene-based quinone-hydroquinone couples, in which they examined the susceptibility of each quinone to a Michael addition or substitution, as well as reversible gem-diol formation. The main conclusion was that as the quinone reduction potentials (and thus electron deficiency or Lewis acidity) increased above 0.9 V vs SHE, the quinones became severely susceptible to irreversible Michael addition/substitution reactions with water. Indeed, they found that almost no quinones exhibited both a reduction potential above 0.9 V, and thermodynamic resistance to Michael addition and/or gem-diol formation. As will be discussed in more detail in the next section, this insight has been strongly supported by the experimental literature, which features significantly more chemically stable quinone-based negolyte reactants (with reduction potentials <0.2 V vs SHE)[53,54,60] than posolyte reactants (with reduction potentials >0.8 V), the most stable of which decomposes at ∼0.5%/day.[61]

Chemical studies have established that nucleophilic reactions occur in other nonquinone-related high-potential substrates as well, such as nitroxide radicals,[62,63] which have reduction potentials around 0.8 V vs SHE, and organometallic complexes based on ferrocene (Fc) or ferrocyanide, which have reduction potentials around ∼0.4−0.6 V. As an example of the former case, electrochemical oxidation of 4-hydroxy-(2,2,6,6 tetramethylpiperidin-1-yl)oxyl (4-HO-TEMPO) results in the formation of 4-HO-TEMPO$^+$, which, in alkaline electrolyte, is highly susceptible to nucleophilic addition of OH^-, which causes progressive acidification of the electrolyte. Acidic conditions lead to 4-HO-TEMPO disproportionation to 4-HO-TEMPO$^+$ and 1,4-dihydroxy-2,2,6,6-tetramethylpiperidine, the latter of which is redox-inactive. Similarly, electrochemical oxidation of Fc and ferrocyanide results in the formation of Fc^+ and ferricyanide, respectively, both of which are prone to nucleophilic attack by OH^-.[64,65] In the case of Fc^+, nucleophilic attack by water may still occur to some extent, even when protective alkyl substituents are used,[66] particularly if those groups are close to the Fc redox center. An example of this is furnished by (ferrocenylmethyl)-trimethylammonium salts, where nucleophilic substitution of the quarternary ammonium group leads to the loss of trimethylamine as a leaving group.[67,68] As water is a weaker nucleophile than OH^-, an important lesson from this work is that aqueous RFB reactants based on nitroxide radicals should ideally be deployed in neutral pH electrolytes, and those based on Fc or ferricyanide should ideally be deployed in neutral-to-weakly alkaline electrolytes.

It is worth noting that some low-potential redox couples may also be prone to decomposition by nucleophilic attack in addition to other mechanisms that may delimit a range of preferred operating conditions. This is the case for methyl viologen (MV), although it has low first and second electron reduction potentials at −0.45 and −0.7 V vs SHE, respectively. The ammonium functional groups in either the fully oxidized (MV^{2+}) or singly reduced ($MV^{\bullet+}$) redox states are vulnerable to OH^- attack, whereas the doubly reduced MV° species has poor water solubility and is prone to protonation under acidic conditions.[69] Even at pH 7, however, dimerization of two monocationic MV^+ radicals can result in the formation of a stable internal charge transfer complex[70] that can then disproportionate into MV^{2+} and MV°,[71,72] resulting in loss of redox activity.

A subset of nucleophilic reactions initiated by water to which aqueous organic RFB reactants are prone is the breakdown, or hydrolysis, of substituents attached to redox-active molecules. Functional groups such as esters, ethers, and amides[73] are particularly vulnerable to this attack, and in some cases, hydrolysis can lead to the collapse of the backbone of the oxidized form of the redox-active molecule, resulting in a complete loss of redox activity. Such collapse can be catalyzed by H^+ or OH^- in acid or alkaline electrolytes, respectively, depending on the nature of the substituent. Hydroxide-initiated hydrolysis of alloxazines such as lumichrome,[74,75] and their tautomer isoalloxazines such as riboflavin,[76−78] has been widely studied. Koziol et al. have shown that under alkaline conditions the uracil ring in lumichrome can be opened through the hydrolysis of amide, leading to the formation of 6,7-dimethy1-3-ureidoquinoxaline-2-carboxylic acid.[74] Riboflavin likewise can undergo ring-opening upon hydrolysis, yielding urea and l,2-dihydro-6,7-dimethyl-2-keto-l-D-ribityl-3-quinoxaline carboxylic acid.[76−78] Although high pH values catalyze amide hydrolysis,[77] the low p*K*a values at the amide nitrogen (8.4 and 11.4 for lumichrome) result in the accumulation of two negative charges in the imidic conjugate system, which lowers the electrophilicity of the carbonyl groups and hinders the attack by OH^-.[74] Introducing electron-donating substituents to organic molecules prone to hydrolysis by OH^- is therefore expected to lower their reactivity, and a computational study suggests that attaching such groups to alloxazines can indeed decrease the electrophilicity of the carbonyl groups and protect against hydrolysis.[79]

The disproportionation of some redox couples can initiate chemical decomposition. Disproportionation is said to occur when two species with identical oxidation states undergo a redox reaction in which one is reduced and the other is oxidized, resulting in two different products, of lower and higher oxidation states, respectively. Capacity fade in an RFB results if either of the products is redox-inactive or is of sufficiently low solubility to precipitate. Moreover, if either product exhibits a more extreme redox potential than the original couple or a similar redox potential with more sluggish kinetics, an apparent capacity fade will be observed for given cycling potential limits. Quinones are susceptible to this mechanism: the disproportionation of anthrahydroquinone (2-electron reduced anthraquinone) to

https://dx.doi.org/10.1021/acs.chemrev.9b00599
Chem. Rev. 2020, 120, 6467−6489

anthrone and anthraquinone was observed during electrochemical reduction of unsubstituted anthraquinone under highly acidic condition.[80] Shi et al. also obtained monomers and dimers of 1,8-dimethoxy-10-anthrone upon chemical reduction of 1,8-dimethoxyanthraquinone with sodium borohydride and trifluoroacetic acid.[81] In agreement with these studies, Goulet and Tong et al.[32] and Jin and Jing et al.[82] have demonstrated the formation of anthrone and its dimer in alkaline and neutral media, respectively, their results are discussed in more detail in the next section.

Tautomerization occurs where there is a formal migration of a hydrogen atom along with an exchange between a single bond and an adjacent double bond without changing the carbon skeleton.[83] Tautomers generally have different thermochemical properties than the original molecule, and if they have sufficiently more extreme reduction potentials or lower solubilities as well, the formation of any such species during electrochemical cycling will result in capacity fade and/or a reduction in cell energy density. Aza-substituted conjugated π-systems based on quinones, viologens, and phenazines are usually susceptible to this transformation during electrochemical cycling.[84] This is because redox reactions of these organic molecules involve the reorganization of conjugated double bonds, and in the course of such rearrangement, a tautomer may be a metastable intermediate. This is not the case for simpler aromatic molecules. Phenols, for example, exist exclusively in the enolic form, as the energy decrease by rearrangement to the tautomeric keto-structure is offset by the simultaneous large decrease in resonance energy.[85] Tautomeric ketonic structures become particularly energetically favorable in naphthoquinones,[86] polyhydric phenols and especially in the hydroxyl derivatives of polycyclic aromatic hydrocarbons.

Understanding the susceptibilities of various classes of aqueous organic species to decomposition mechanisms discussed above is critical to devising molecular engineering strategies for enhancing RFB reactant stability. This is also important because decay rates may increase with reactant concentration for certain chemistries, such as those subject to bimolecular decomposition pathways (e.g., disproportionation and dimerization). Because practical RFBs would ideally operate at high reactant concentrations in order to achieve high energy densities, any trade-off between energy density and stability must be well understood. In general, quantitative correlation of capacity fade measured at the cell level to particular decomposition mechanisms is an important research task and, where it has occurred, is highlighted in this review.

2.2. Electrochemical Assessments of Full Cell Capacity Fade

Electrochemical measurements involving redox reactions at an electrode are a natural way to probe the chemical stability of a redox couple in both its oxidized and reduced forms. A classic means of doing this is via cyclic voltammetry (CV), in which the reversibility of the current passed at the electrode during cyclic potential sweeps is a direct indication of the chemical stability of the oxidized and reduced forms of the redox couple involved.[87] Given the sensitivity of CV measurements, the longest time scales for chemical decay for which CV-based analysis of bulk concentrations can be used are, however, much shorter (on the order of minutes) than typical time scales for aqueous RFB reactant stability (hours to days). Thus, bulk electrolysis in flow cells is by far the most common technique used to assess chemical stability—here, Coulombic capacity upon oxidation and reduction of the entire electrolyte is a proxy for concentration of redox-active reactants, and repeated reduction—oxidation cycling is a means to assessing average RFB chemical lifetime. The fraction of negolyte (posolyte) active species in the reduced (oxidized) state is often referred to as the state of the charge (SOC) of the electrolyte.

In most studies, flow cells comprising two electrolytes separated by an ion-exchange membrane are used for capacity fade analysis. The reactant of interest is typically dissolved in the capacity-limiting side (CLS) or electrolyte, whereas the noncapacity-limiting side (NCLS) contains a counter electrolyte with a higher initial Coulombic capacity. It is important that the NCLS have excess capacity for discharging as well as for charging, so that small amounts of side reactions such as hydrogen evolution or oxygen evolution, as well as degradation of the active species itself, do not cause the NCLS to reach its capacity limit. Where the NCLS comprises a different redox couple than that in the CLS, the setup (hereafter referred to as the "full cell" setup) mimics the basic unit of an actual RFB (Figure 1a). The current efficiency of a full cell is often evaluated as the ratio of the discharge duration to the immediately preceding charging duration in a galvanostatic charge−discharge cycle. Any nonrecoverable capacity losses originate from decomposition of redox-active material in the CLS, provided electrolyte leakage and permeation across the membrane, the latter of which increases with concentration,[37] do not occur to any appreciable extent.[88] Limiting unwanted current efficiency and capacity losses via ingress of atmosphere, electrolyte leakage, or electrolyte permeation through the membrane by using properly sealed plumbing and/or testing the flow cell in a glovebox, as well as judicious choice of membrane[37] are therefore critical to proper evaluation of the stability of RFB chemistries.

The influence of cycling protocol on the measured capacity fade rate, and how it may differ from the actual fade in Coulombic capacity of the electrolyte, is an underappreciated issue. Constant-current (galvanostatic) cycling, where each reduction/oxidation half-cycle ends when a prescribed cell overpotential is reached, is performed in most studies. However, because of high mass transport overpotentials at extreme SOC values, as well as the time lag between the attainment of a particular SOC value in the cell and its attainment in the reservoirs, less than 100% of the actual capacity is accessed before the switching occurs,[33,89] with this apparent capacity dropping with increasing current density. Consequently, transient changes in membrane resistance or surface exchange kinetics, caused by temperature variations, membrane aging, or other time-varying environmental factors, can result in corresponding changes to apparent capacity, although the actual electrolyte capacity may remain unchanged and accessible via other cycling regimens. These spurious changes in apparent capacity are typically a negligible fraction of the actual electrolyte capacity but become more important for chemically stable electrolytes where capacity fade from molecular decomposition is comparably small. A more rigorous technique for interrogating actual capacity is constant-potential, or potentiostatic, cycling, where each half-cycle ends only after the reduction/oxidation current has become negligible, at which point close to 100% of the available charge is expected to have been extracted. This is strictly true if the chosen potential limits provide large enough overpotentials to access essentially 100% of the electrolyte capacity and side reactions at those limits are negligible. Equally effective is galvanostatic cycling in which each half-cycle is followed by a potential hold until the current has

https://dx.doi.org/10.1021/acs.chemrev.9b00599
Chem. Rev. 2020, 120, 6467−6489

Table 1. Summary of Results from Full Cells Containing Quinone-Based Reactants in the CLS[a]

name	author/year	capacity fade rate		electron conc. (M)	redox potential (V vs SHE)	pH
		%/cycle	%/day			
DMBQ/ $K_4Fe(CN)_6$	Sun/2019[35]	0.11	22	0.2	**−0.75**/0.50	14
DMOBQ/$K_4Fe(CN)_6$		0.17	35	0.2	**−0.70**/0.50	14
DHBQ/$K_4Fe(CN)_6$	Yang and Tong/2018[36]	0.24	9	1	**−0.72**/0.50	14
DHAQ/$K_4Fe(CN)_6$	Lin/2015[11]	0.1	8	1	**−0.68**/0.50	14
	Goulet and Tong/2019[32]		**0.14**	0.18	**−0.68**/0.50	14
bislawsone/$K_4Fe(CN)_6$	Tong/2019[98]	**0.038**	**0.74**	2	**−0.55**/0.50	14
2,6-DBEAQ/$K_4Fe(CN)_6$	Kwabi and Lin/2018[53]	**0.001**	**0.04**	1	**−0.54**/0.50	12
2,3-HCNQ/$K_4Fe(CN)_6$	Wang/2018[100]	0.053	3.4	0.5	**−0.53**/0.50	14
2,6-DPPEAQ/$K_4Fe(CN)_6$	Ji/2018[54]	**0.0004**	**0.014**	1	**−0.47**/0.50	9−13
PEGAQ/$K_4Fe(CN)_6$	Jin and Jing/2019[82]	**0.04**	**0.5**	3	**−0.43**/0.50	7
ARS/BQDS	Zhang/2015[102]	2	16	0.1	**0.08**/0.91	0
AQS/HBr	Gerhardt/2017[52]	1	19	2	**0.19**/1.06	0
AQDS/HBr	Huskinson/2014[60]	0.014	0.19	2	**0.21**/1.06	0
	Chen/2016[88]	0.1	1.2	2	**0.21**/1.06	0
$Zn(OH)_4^{2-}$/FQH_2	Park/2019[103]	0.09	2.5	0.2	−1.30/**0.70**	**-0.7**
AQDS/**DHDMBS**	Hoober-Burkhardt/2017[96]	1	3.5	2	0.21/**0.82**	0

[a]Capacity fade results established by potentiostatic cycling or galvanostatic cycling with potentiostatic finishes, are marked in bold text, whereas apparent capacity fade results from purely galvanostatic cycling are left in plain text. In the "name" field, the active reactant in the negolyte is on the left and that for the posolyte is on the right. The CLS is marked out in bold, whereas the NCLS is in plain text. "electron conc." refers to moles of transferrable electrons per liter of electrolyte. "redox potential" refers to redox couple in the CLS (bold), and that of the NCLS (plain text). DMOBQ = 2,5-dimethoxy-3,6-dihydroxy-1,4-benzoquinone, DMBQ = 2,5-dimethyl-3,6-dihydroxy-1,4-benzoquinone, DHBQ = dihydroxybenzoquinone, DHAQ = 2,6-dihydroxanthraquinone, 2,6-DBEAQ = 4,4′-((9,10-anthraquinone-2,6-diyl)dioxy)dibutyrate, 2,3-HCNQ = 2-hydroxy-3-carboxy-1,4-naphthoquinone, 2,6-DPPEAQ = (((9,10-dioxo-9,10-dihydroanthracene-2,6-diyl) bis(oxy))bis(propane-3,1-diyl))bis(phosphonic acid), PEGAQ = 1,8-bis(2-(2-(2-hydroxyethoxy)ethoxy)ethoxy)anthracene-9,10-dione, ARS = 3,4-dihydroxy-9,10-anthraquinone-2-sulfonic acid, AQS = anthraquinone monosulfonic acid, AQDS = anthraquinone disulfonic acid, FQH_2 = 2,3,5,6-tetrakis((dimethylamino)methyl)hydroquinone, DHDMBS = 3,6-dihydroxy-2,4-dimethylbenzenesulfonic acid.

become negligible or in which capacity is assessed only in occasionally inserted potentiostatic cycles.[33,90] To demonstrate the vulnerability of galvanostatic cycling results to misinterpretation, Goulet and Aziz[33] inserted and removed a series resistance equivalent to a 25% increase in cell resistance into a cycling experiment, demonstrating artificial increases and decreases in apparent capacity from galvanostatic cycling measurements, and demonstrating the absence of such an artifact in potentiostatic or combined potentiostatic-galvanostatic cycling. Henceforth, we use the term "apparent capacity" to describe the result of galvanostatic cycling without potential holds.

Table 1 summarizes temporal and cycle-based capacity fade rates of some recently reported aqueous organic full cells where the CLS contains a quinone-based redox couple. High-potential redox couples based on benzoquinone were among the first[91−94] reactants studied for aqueous flow batteries, and in recent years, considerable effort has been put into developing chemically stable low-[53,54] and high-potential[61,95−97] quinone-based redox couples. There is no correlation between cyclic and temporal fade rates in Table 1. This indicates that widely differing cycle periods (which are functions of the applied current, reactant concentration and electrolyte volume) have been used in the literature, and that full cell chemistries with low fade rates per cycle will not necessarily have a long RFB calendar lifetime, particularly in practical deployment, where cycle periods are likely to be much longer than in published research. It is important to note that, for all aqueous organic electrolytes for which we have observed sufficient experimentation to distinguish between cycle-denominated fade and time-denominated fade, it has been found that the amount of lost capacity is essentially independent of the number of charge−discharge cycles to which a species is subjected: the amount of lost capacity depends only on the passage of time, although the rate can depend on molecular concentrations, pH, and SOC.[32,33,54,82,90] It is also worth noting that galvanostatic cycling was used to assess capacity retention in all but five[32,53,54,98,99] of these studies. However, given that the vast majority of reported fade rates are above 0.1%/day (which extrapolates to 36.5%/year assuming a constant fade rate),[35,36,52,60,61,82,96,100] it is likely that much of that apparent capacity fade is a consequence of molecular decomposition rather than of the artifacts to which galvanostatic cycling is vulnerable.

Understanding how capacity fade rates can be quantitatively attributed to specific decomposition mechanisms can inform mitigation strategies. A notable example of such an exercise is the work of Narayanan and co-workers regarding the development of a benzoquinone -based posolyte for aqueous organic RFBs.[61,95,96] They first demonstrated the feasibility of operating an aqueous organic RFB with 4,5-dihydroxybenzene-1,3-disulfonic acid (BQDS), also known as tiron, in the posolyte and either anthraquinone-2-sulfonic acid (AQS)[101] or anthraquinone-2,6-disulfonic (AQDS)[95] acid in the negolyte.

The hydrophilic, electron-withdrawing sulfonic acid groups on BQDS were found to confer on it a high solubility (~4 M) and a relatively high reduction potential (0.85 V vs SHE), yielding full-cell potentials of 0.65 and 0.80 V when paired against AQDS and AQS, respectively. Galvanostatic cycling of a capacity-balanced AQDS/BQDS cell yielded a very high apparent capacity fade rate (50% capacity loss after the first cycle), after which the authors conducted chemical analysis of cycled electrolytes using proton nuclear magnetic resonance (NMR) spectroscopy.[95] Significant molecular changes were observed only in the posolyte, which led to the hypothesis, in agreement with previous work,[91] that the ortho-quinone resulting from electrochemical oxidation of BQDS was subject

https://dx.doi.org/10.1021/acs.chemrev.9b00599
Chem. Rev. 2020, 120, 6467−6489

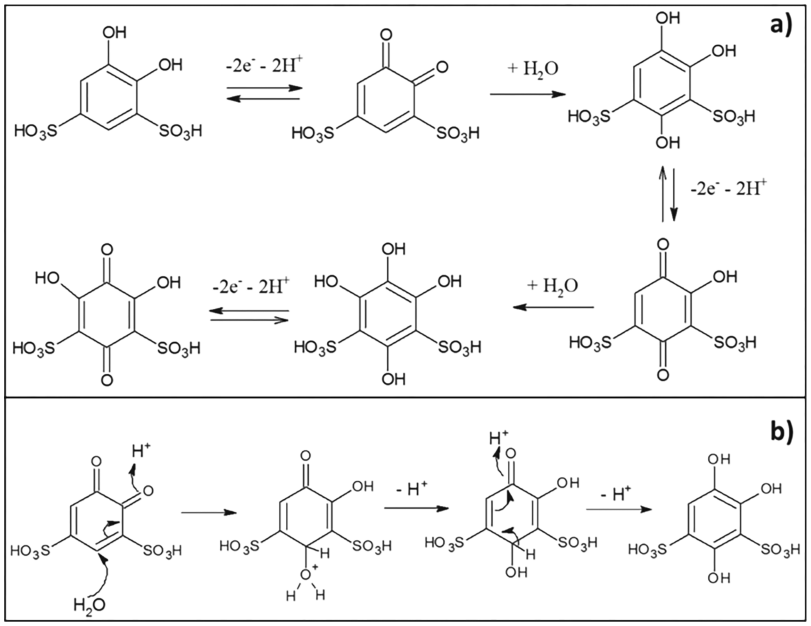

Figure 3. (a) Schematic of the transformation of BQDS during charging; (b) schematic of the Michael reaction showing the nucleophilic addition of water to the ortho-quinone resulting from BQDS oxidation. Reprinted with permission from ref 95. Copyright 2016 Electrochemical Society.

to chemical reduction via the Michael addition of water. Two successive electrochemical oxidation and Michael addition reactions eventually result in the formation of a fully substituted para-benzoquinone with two electron-donating hydroxyl groups,[104] and a correspondingly lower redox potential (~0.65 V vs SHE) than the original redox couple (Figure 3).

These transformations led to the negolyte becoming capacity-limiting, as three equivalents of AQDS were required to completely convert every equivalent of BQDS to its final form. Moreover, the electron-donating hydroxyl substituents introduced by Michael reactions decreased the reduction potential of the molecule, cutting the overall cell voltage to less than 0.5 V.

To mitigate the Michael reaction, Narayanan and co-workers designed a new redox couple based on 3,6-dihydroxy-2,4-dimethylbenzenesulfonic acid (DHDMBS).[96] This molecule features two moderately electron-donating methyl groups (as opposed to strongly electron-donating hydroxyl groups) and one electron-withdrawing sulfonic acid group and had a relatively high redox potential (0.82 V vs SHE) and solubility (2 M in 1 M H_2SO_4). However, because the methyl groups lower the electrophilicity of the only unsubstituted position, which is itself adjacent to one of the bulky methyl groups, DHDMBS was hypothesized to be less sterically and energetically prone to Michael reaction compared to BQDS upon electrochemical oxidation. Indeed, in an AQDS/DHDMBS flow cell, DHDMBS did not show any noticeable chemical decomposition for 25 cycles, although there was significant apparent capacity fade, at a rate of 5.5%/day. This was attributed to a combination of DHDMBS crossover through the Nafion membrane and its slow desulfonation by hydrolysis of the sulfonic acid, the latter of which causes capacity fade via removal of the solubilizing sulfonic acid group on DHDMBS, and thus loss of redox-active material from solution through precipitation. In a subsequent publication,[61] crossover and proto-desulfonation were disambiguated using a combination of a low-permeability sulfonated polyether ether ketone-based membrane and a symmetric cell protocol (discussed in more detail in the next section), in which both electrolytes comprised DHDMBS and AQDS. This protocol substantially reduced DHDMBS crossover, and allowed direct interrogation of the influence of desulfonation on the apparent capacity fade rate, which turned out to be about 0.48%/day in the absence of sulfuric acid.

It is notable that DHDMBS, as a rationally designed posolyte reactant, is the only quinone-based species with a redox potential above 0.8 V vs SHE that exhibits moderate stability (between 0.1 and 1%/day) or better upon electrochemical cycling. That high-potential benzoquinone-based reactants have generally not exhibited high long-term chemical stability[91,92,103,105,106] amounts to experimental validation of previously discussed theoretical calculations[59] suggesting that quinones become more susceptible to Michael addition/substitution reactions as their reduction potentials increase. Indeed, particularly direct experimental evidence has been furnished for this conclusion in a recent study by Preger et al.,[107] in which the chemical stability of several benzoquinone-derived molecules was evaluated, and they found a strong inverse correlation between quinone half-life and reduction potential.

A consequence of this trend is that considerably more success has come from the development of quinone-based negolytes, which are often paired with high-potential inorganic redox couples (chiefly based on bromine or ferrocyanide in acidic or basic conditions, respectively) in full cells. The first of such negolyte reactants was anthraquinone-2,7-disulfonic acid (AQDS),[60] which exhibited an apparent capacity fade rate of 0.2%/day in a full cell with a hydrobromic acid posolyte. There is some ambiguity regarding the mechanism of full redox access of the theoretical 2-electron Coulombic capacity of AQDS. On the basis of nuclear magnetic resonance (NMR), CV, and bulk electrolysis measurements, Carney[108] and Wiberg[109] and co-workers have suggested that reversible intermolecular dimerization of AQDS occurs at solution concentrations greater than 10 mM, which inhibits full 2-electron electrochemical reduction or reduction using chemical oxidants. Carney et al.[108] speculated that CO_2 is bound in a 1:1 anthraquinone-CO_2 adduct in bulk AQDS powder. Upon dissolution in acidic electrolyte, the

https://dx.doi.org/10.1021/acs.chemrev.9b00599
Chem. Rev. 2020, 120, 6467−6489

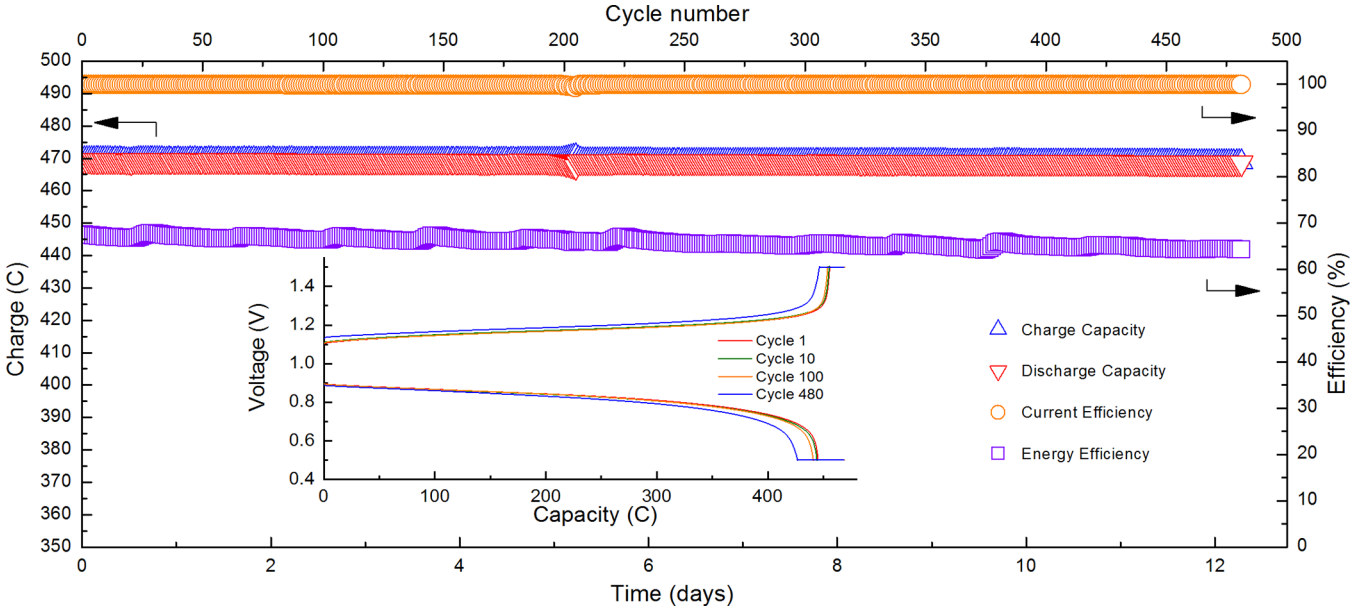

Figure 4. Current efficiency (circles), energy efficiency (squares), charge (upward-pointing triangles) capacity, and discharge (downward-pointing triangles) capacity versus time and cycle for a full cell comprising 5 mL of 0.5 M 2,6-DPPEAQ at pH 9 in the negolyte, and 80 mL of 0.4 M potassium ferrocyanide and 0.1 M potassium ferricyanide at pH 9 in the posolyte. The cell was cycled galvanostatically at 100 mA/cm^2 between 1.5 and 0.5 V and each half-cycle ended with a potentiostatic hold until the magnitude of the current density fell below 2 mA/cm^2. Inset: capacity versus cell voltage at the 1st, 10th, 100th, and 480th cycle. Adapted with permission from ref 54. Copyright 2019 John Wiley and Sons.

AQDS-CO_2 adduct would be hydrolyzed to form semianthraquinone, which would then dimerize into semianthraquinone−anthraquinone units with an overall Coulombic capacity of 1.5 electrons per molecule of AQDS. In neutral to basic pH, they expect that hydroxyanthraquinone−anthraquinone dimers would be formed, resulting in an overall capacity of one electron per molecule of AQDS. The universality of this capacity-restriction mechanism is however in doubt, as Chen et al. accessed over 95% of the theoretical capacity of AQDS in an acidic AQDS/Br cell.[88] Such a high capacity is consistent with a number of other reports of acidic,[110] neutral,[82] and alkaline[33] AQDS or anthraquinone-based chemistries in which electrochemical access of ≥90% of the full 2-electron Coulombic capacity has been demonstrated.

Several studies have explored the use of AQDS and its derivatives[52,110] in full cells as a platform for mechanistic analysis of current−voltage relationships in RFBs,[88] partitioning voltage losses within the full cell stack,[89] and demonstrating the feasibility of RFBs charged by solar cells.[111−113] However, beyond the contribution of bromine crossover,[88,114] the origin of capacity fade in AQDS/Br cells has not been investigated in detail, although hydroxylation,[110] and disproportionation[108] of the reduced anthrahydroquinone to anthraquinone and redox-inactive anthrone, have been hypothesized.

Owing in part to potential safety issues raised by the use of bromine in acidic AQDS-Br full cells, and the facile crossover of uncharged Br_2 species across most ion-exchange membranes, 2,6-dihydroxyanthraquinone (DHAQ) was developed as an alternative negolyte reactant at pH 14 and demonstrated in a full cell against a posolyte comprising potassium ferrocyanide.[11,115] A capacity fade rate of 8%/day was observed, and was attributed to molecular decomposition in a subsequent study.[33] By jointly using electrochemical cycling and chemical analysis, Goulet and Tong et al.[32] quantitatively demonstrated that progressive loss of capacity during DHAQ cycling is primarily due to the disproportionation of 2-electron-reduced DHAQ followed by the formation of an anthrone dimer, which is redox-inactive. Interestingly, in the case of 2,6-dihydroxyanthrone (DHA) formation at pH 14, capacity recovery is possible because DHA can be reoxidized to DHAQ under aerobic conditions. Even in the presence of oxygen, however, such recovery is only partial, because DHA irreversibly converts to its dimer, $(DHA)_2$. The first demonstration of the recovery effect, by Goulet and Tong et al.,[32] showed a recovery of 70% of the lost capacity. Because $(DHA)_2$ has a higher reduction potential, has a 2-fold lower specific capacity than DHAQ, and is unstable at pH 14, some capacity loss is unavoidable. It was hypothesized that minimizing anthrone formation by avoiding a high concentration of reduced species, or high SOC, during cycling would reduce the capacity fade rate of a DHAQ-based cell. Consistent with this hypothesis, restricting the maximum SOC from ∼100% to 88% cut the capacity fade rate by almost 2 orders of magnitude, from 5.6%/day to 0.14%/day without utilizing the recovery effect.

Computational chemistry indicates that the propensity for anthrahydroquinones to disproportionate into the corresponding anthrone and anthraquinone correlates inversely to the reduction potential of the anthraquinone.[32] This result is consistent with a recent study showing that a full cell featuring a negolyte with polyethylene glycol-functionalized anthraquinone (PEGAQ), with a higher reduction potential than DHAQ, exhibits a slower capacity fade rate from anthrone and anthrone dimer formation.[82] Specifically, PEGAQ at pH 7 has a 250 mV higher reduction potential than DHAQ at pH 14, but a capacity fade rate about 10 times smaller, at 0.5%/day.[82] It is interesting to note that a number of full cells with benzoquinone reactants[35,36] of lower reduction potentials than DHAQ exhibit accordingly greater capacity fade rates, up to 35%/day in one case. However, the degree to which these higher capacity fade rates reflect higher rates of formation of anthrone-like species is an open question, requiring quantitative study of the correlation between capacity fade and chemical decay and controlling for pH.

https://dx.doi.org/10.1021/acs.chemrev.9b00599
Chem. Rev. 2020, 120, 6467−6489

Table 2. Summary of Results from Full Cells Containing Viologen, Nitroxide Radical and Iron Coordination Complex-Based Reactants[a]

name	author/year	capacity fade rate		electron conc. (M)	redox potential (V vs SHE)	pH
		%/cycle	%/day			
Diquat 5/FcNCl	Huang/2018[128]	0.2	0.8	0.5	−0.51/0.61	7
MV/4-HO-TEMPO	Liu/2015[62]	0.1	27.5	0.5	−0.45/0.80	7
$(NPr)_2TTZ/N^{Me}$-TEMPO	Luo/2018[122]	0.03	2.25	0.1	−0.44/1.00	7
MV/TEMPO polymer	Janoschka/2015[120]	0.25	7.5	0.37	**−0.45**/0.90	7
MV/TEMPTMA	Janoschka/2016[121]	0.026	0.27	2	−0.45/1.00	7
$(SPr)_2V$/KI	DeBruler/2018[127]	0.01	0.45	0.5	**−0.43**/0.57	7
BTMAP-Vi/BTMAP-Fc	Beh/2017[90]	**0.0057**	**0.1**	1.3	−0.36/0.39	7
BTMAP-Vi/**BTMAP-Fc**		**0.0011**	**0.033**	1.0	−0.36/0.39	7
$(NPr)_2V$/FcNCl	DeBruler/2017[129]	0.01	0.5	0.5	(−0.35,−0.72)/0.61	7
$(NPr)_2V$/N-Me-TEMPO	Hu/2018[130]	0.005	0.2	0.5	−0.38/1.00	7
$[(Me)(NPr)V]Cl_3$/FcNCl	DeBruler/2017[129]	0.18	8.8	0.5	(−0.39,-0.78)/0.61	7
MV/FcNCl	Hu/2017[125]	0.01	0.22	0.5	−0.45/0.61	7
Phenazine-TEMPO combimolecule	Winsberg/2016[119]	0.011	0.62	0.01	−0.39/0.81	7
Zn^{2+}/**g+-TEMPO**	Chang/2017[117]	0.046	0.7	0.2	−0.69/**0.81**	7
BTMAP-Vi/**TMAP-TEMPO**	Liu/2019[118]	0.007	0.6	0.1	−0.38/**0.81**	7
		0.015	0.55	1.5	−0.38/**0.81**	7
Zn^{2+}/**SO_4-TEMPO**	Winsberg/2017[124]	0.0058	1.38	0.035	−0.87/**0.82**	7
Zn^{2+}/**Im-TEMPO**	Chang/2019[123]	0.11	21.2	0.4	−0.69/**0.95**	7

[a]Capacity fade results established by potentiostatic cycling or galvanostatic cycling with potentiostatic finishes are marked in bold text, whereas apparent capacity fade results from purely galvanostatic cycling are left in plain text. In the "name" field, the active reactant in the negolyte is on the left and that for the posolyte is on the right. Where there is a CLS, the reactant it contains is marked out in bold, whereas in capacity-balanced configurations, both reactants are in plain text. "electron conc." refers to moles of transferrable electrons per liter in the CLS. "redox potential" refers to redox couple(s) in the negolyte (left), and that of the posolyte (right), with the CLS marked out in bold. We include hybrid flow/non-flow batteries with zinc electroplating when the flowing aqueous organic is the capacity-limiting side or is believed to be the capacity-limiting side after capacity fade begins. MV = methyl viologen, 4-HO-TEMPO = 4-hydroxy-2,2,6,6-tetramethylpiperidin-1-oxyl, $(NPr)_2TTZ$ = 4,4′-(thiazolo[5,4-*d*]thiazole-2,5-diyl)bis(1-(3-(trimethylammonio)propyl)pyridin-1-ium) tetrachloride, N^{Me}-TEMPO = 4-trimethylammonium-TEMPO, $(SPr)_2V$ = 1,1′-bis(3-sulfonatopropyl)-4,4′-bipyridinium, FcNCl = ferrocenylmethyl)trimethylammonium chloride, BTMAP-Vi = bis(3-trimethylammonio)-propyl viologen tetrachloride, BTMAP-Fc = bis((3-trimethylammonio)propyl)ferrocene dichloride, $(NPr)_2V$ = 1,10-bis[3-(trimethylammonio)-propyl]-4,40-bipyridinium tetrabromide, (Me)(NPr)V = 1-methyl-10-[3-(trimethylammonio)propyl]-4,40-bipyridi-nium trichloride, g+-TEMPO = glycidyltrimethylammonium cation-grafted TEMPO, TMAP-TEMPO = 4-[3-(trimethylammonio)propoxy]-2,2,6,6-tetramethylpiperidine-1-oxyl, SO_4-TEMPO = TEMPO-4-sulfate potassium salt, TEMPTMA = *N*,*N*,*N*-2,2,6,6-heptamethylpiperidinyl oxy-4-ammonium chloride, Im-TEMPO = imidazolium-grafted TEMPO.

A recent detailed study by Tong et al.[98] of the dimerized naphthoquinone bislawsone in an alkaline cell has demonstrated that tautomerization, rather than disproportionation, of the hydroquinone chiefly accounts for molecular decomposition-induced loss in cell capacity. The correlation between tautomerization of the hydroquinone to insoluble and/or redox-inactive di- and tetra-ketone forms and capacity fade was supported in similarly quantitative fashion to an earlier study on DHAQ decomposition: by comprehensive electrochemical cell cycling and post mortem chemical analysis of the electrolyte via NMR and high-resolution high-performance liquid chromatography (HPLC). Theoretical calculations suggest that naphthoquinone susceptibility to tautomerization generally increases with reduction potential but is also highly sensitive to functionalization—in particular, the calculations suggest that oxy-alkyl substitutions impart greater protection against tautomerization than the hydroxyl groups in bislawsone. Although it is possible that tautomerization is universally responsible for capacity fade in naphthoquinones, corroboration is difficult given the paucity of publications in this area.[100,104] Other hypotheses have been proposed, such as nucleophilic attack either directly by OH^-, or after quinone epoxidation from hydroperoxides created in the presence of trace amounts of oxygen.[104]

Notwithstanding these uncertainties, alkaline flow cells utilizing negolytes featuring quinones with reduction potentials at least 100 mV higher than that of DHAQ and oxy-alkyl substitutions (i.e., to limit both anthrone formation and tautomerization) have exhibited among the lowest capacity fade rates reported in the literature.[53,54] Indeed, the current record for the lowest demonstrated capacity fade rate for any flow battery, organic or inorganic, in the absence of electrolyte rebalancing processes belongs to one with a phosphonate-functionalized anthraquinone (2,6-DPPEAQ) in the negolyte and a $K_4Fe(CN)_6$ posolyte, at 0.014%/day according to galvanostatic cycling with potential hold finishes (Figure 4).[54]

A full cell based on a carboxylate-functionalized analogue of 2,6-DPPEAQ (2,6-DBEAQ) exhibited a higher capacity fade rate, at 0.04%/day.[53] At such low fade rates (≤0.1%/day), the measured fade rate is often associated with a high relative experimental uncertainty, as it is highly sensitive to small changes in the rates of negolyte leakage and crossover through pinholes in the membrane. Purely galvanostatic cycling is unlikely to provide an assessment of the actual capacity fade rate, as the apparent capacity would be highly sensitive to fluctuations caused by diurnal temperature changes and drifts in membrane resistance. Additionally, discerning the origins of capacity fade becomes challenging, as several weeks to months of testing at room temperature would be required to accrue enough decomposed material for meaningful chemical analysis (e.g., using NMR and HPLC). Consequently, chemical analysis of 2,6-DBEAQ and 2,6-DPPEAQ after accelerated chemical

https://dx.doi.org/10.1021/acs.chemrev.9b00599
Chem. Rev. 2020, 120, 6467−6489

decomposition by storage at elevated temperatures in both redox states was used to determine decomposition pathways at different pH values. The suggestion from these studies was that whereas nucleophilic substitution by OH^- was the dominant decay mechanism for both quinones at pH 14, an intramolecular reaction with carboxylate acting as the nucleophile dominates in the decomposition of 2,6-DBEAQ and no analogous intramolecular reaction of 2,6-DPPEAQ was observed at pH 12 at elevated temperatures due to a much weaker nucleophilicity of the bulky phosphonate group relative to carboxylate.[116]

In comparison to much of the RFB literature involving quinones, the details of molecular decomposition-induced capacity fade in most full flow cell reports with nitroxide radical,[62,117−124] iron coordination complex,[90,125,126] and viologen-based[62,90,122,127−130] reactants are less understood. This is in large part because most full cell studies featuring these species (Table 2) do not report a CLS. Thus, because initial Coulombic capacities of the negolyte and posolyte are nominally identical, it is impossible, in the absence of other information about the electrolyte chemistries, to pinpoint the decomposing electrolyte. In principle, one may avoid this shortcoming via chemical analysis of both cycled electrolytes; however, such analysis is valid only if molecule crossover and electrolyte leakage are properly accounted for.

Because viologens and ferrocene/nitroxide-radical based reactants tend to have low (∼−0.4 V vs SHE) and high (∼0.4−1.0 V vs SHE) redox potentials, respectively, they are often paired as negolyte/posolyte combinations in full cells, with maximum full cell voltages (1.2−1.4 V) approaching the thermodynamic stability window for water.[62,118,120−122,127,130] This pairing is particularly appropriate, as these redox couples are highly chemically unstable under corrosive conditions, i.e., vulnerable, in the oxidized state, to nucleophilic attack by OH^- under alkaline conditions,[63,65] and, in the reduced state, to protonation in acid; consequently in organic RFBs they are used only under neutral conditions. Nevertheless, moderate to high capacity fade rates have been reported in the literature. In the first such study of a viologen/nitroxide-radical full cell in water, Janoschka et al.[120] deployed polymerized MV and TEMPO in a flow cell. Because of the macromolecular nature of the reactants used, the viscosity restricted the concentration to well below the solubility limit, but they were able to use a low-cost microporous separator rather than an ion-selective membrane. The flow cell exhibited an apparent capacity fade rate of 0.75%/day.

The vast majority of other full cell reports based on this motif have used monomeric reactants. Liu et al.[62] reported a water-based methyl viologen/4-HO-TEMPO flow cell with an anion-exchange membrane, and an apparent capacity fade rate equivalent to ∼28%/day; however, the cell was capacity-balanced, and no chemical analysis on cycled electrolytes was performed. DeBruler et al.[129] subsequently reported an apparent capacity fade rate of ∼50%/day for a full cell in which both MV and TEMPO were functionalized with ammonium substituents, yielding 1,10-bis[3-(trimethylammonio)propyl]-4,40-bipyridinium ($(NPr)_2V$) and 4-trimethylammonium-TEMPO (N^{Me}-TEMPO), respectively. During the cycling, they accessed the second reduction of $(NPr)_2V$ at −0.75 V vs SHE, resulting in a higher specific capacity and average full cell voltage than that of the one-electron MV/TEMPO flow cell. The use of charged substituents was meant to prevent dimerization and precipitation of the singly and doubly reduced $(NPr)_2V$, respectively. However, a higher apparent capacity fade rate was exhibited by the $(NPr)_2V/N^{Me}$-TEMPO cell than the MV/4-HO-TEMPO cell, presumably because the two-electron-reduced viologen core in the former is more chemically unstable than the one-electron version.[33,70]

The extent to which this hypothesis explains capacity fade cannot be discerned from these results, because the cell was capacity-balanced and no chemical analysis was performed on cycled electrolytes. Replacing the TEMPO posolyte with one containing an ammonium-substituted Fc complex ((ferrocenylmethyl)trimethylammonium chloride, FcNCl)[129] resulted in a drastic reduction in the apparent capacity fade rate, to 0.5%/day. A reasonable inference from this result is that the redox couple associated with N^{Me}-TEMPO is more chemically unstable than that of $(NPr)_2V$. However, this is apparently contradicted by a subsequent publication in which Hu et al.[130] show that accessing only the first reduction of $(NPr)_2V$ in a capacity-balanced $(NPr)_2V/N^{Me}$-TEMPO full cell results in an even lower apparent capacity fade rate of 0.2%/day, whereas it should be at least 50%/day if N^{Me}-TEMPO were the capacity-limiting reactant. These ambiguities underscore the need for establishing quantitatively rigorous relationships between capacity fade and molecular decay or crossover through the membrane, where applicable.

A significant step toward this goal was taken by Beh et al.,[90] who demonstrated extremely low capacity fade rates (≤0.1%/day) in ammonium-functionalized viologen (Vi)/Fc full cells and provided evidence that capacity fade is attributable to bimolecular decomposition reactions. In their configuration, both Vi and Fc were functionalized with positively charged quaternary ammonium groups, yielding bis(3-trimethylammonio)propyl viologen (BTMAP-Vi), which is identical to $(NPr)_2V$, and bis((3-trimethylammonio)propyl)ferrocene (BTMAP-Fc), respectively. Conventional galvanostatic cycling indicated a higher apparent capacity fade rate than that from potentiostatic cycling; this observation was attributed to a slow increase in membrane resistance. The apparent capacity also exhibited diurnal, cyclic variations due to changes in ambient temperature. Both of these observations underscore the increasing unreliability of purely galvanostatic cycling as a guide to measuring the actual cell capacity fade rate as it approaches 0.1%/day from above.

Potentiostatic cycling of a BTMAP-Vi/BTMAP-Fc cell yielded a temporal capacity fade rate of 0.1%/day for a capacity-balanced cell with reactant concentrations of 1.3 M. This temporal rate was found to be essentially independent of cycle period, indicating that capacity fade was primarily time-denominated (i.e., driven by molecular decomposition or crossover) rather than cycle-denominated. A record low fade rate of 0.033%/day for a BTMAP-Fc-limited cell with BTMAP-Fc concentration of 1.0 M was also found and, based on *ex situ* membrane permeability measurements, about half of the overall capacity fade was attributed to reactant crossover. That the temporal capacity fade rate increases with concentration both in this study and earlier reports on Vi/Fc or TEMPO-based chemistries[62,125] provides support for the interpretation that capacity fade originates in large part from bimolecular reactions between reactants. Taken together, these data are consistent with the notion that capacity fade occurs at a significantly slower rate with ammonium-functionalized reagents owing to increased Coulombic repulsion afforded by the charged substituents. Further corroboration in the case of BTMAP reagents was challenging because, given the fade rates and experimental run times in the study, total capacity fade is on the order of ∼0.1−1% only, which approaches the sensitivity of conventional chemical

https://dx.doi.org/10.1021/acs.chemrev.9b00599
Chem. Rev. 2020, 120, 6467−6489

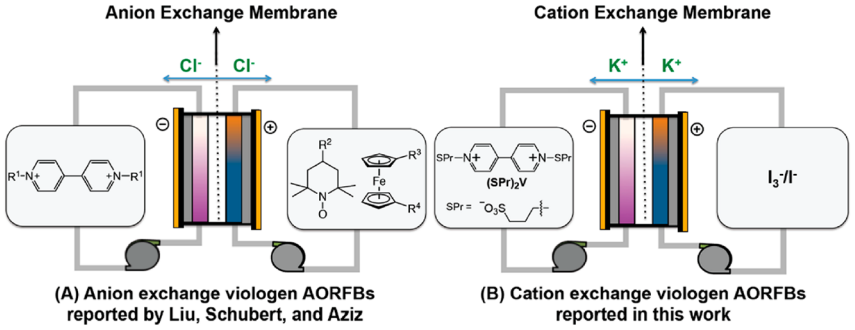

Figure 5. RFB design of (a) anion-exchange viologen/TEMPO and viologen/Fc chemistries and (b) cation-exchange $(SPr)_2V$/iodide chemistry. Reprinted with permission from ref 127. Copyright 2018 American Chemical Society.

Table 3. Summary of Full Cell Results with Aza-Aromatic Reactants[a]

		capacity fade rate				
name	author/year	%/cycle	%/day	electron conc. (M)	redox potential (V vs SHE)	pH
DHPS/$Fe(CN)_6$	Hollas/2018[34]	0.02	0.68	2.8	**−0.81**/0.50	14
ACA/$Fe(CN)_6$	Lin/2016[79]	0.013	1.2	1.0	**−0.62**/0.50	14
FMN/ $Fe(CN)_6$	Orita/2016[139]	0.02	0.6	0.48	**−0.5**/0.50	14
V^{3+}/**MB**	Zhang/2019[145]	0.074	0.76	3.0	−0.26/**0.57**	−0.5

[a]All apparent capacity fade results were obtained by purely galvanostatic cycling. In the "name" field, the active reactant in the negolyte is on the left and that for the posolyte is on the right. The CLS is marked out in bold and the NCLS is in plain text. "electron conc." refers to moles of transferrable electrons per liter of electrolyte. "redox potential" refers to the redox couple in the negolyte (left), and that of the posolyte (right), with the CLS marked out in bold. DHPS = dihydroxyphenazine sulfonic acid, ACA = alloxazine 7/8-carboxylic acid, FMN = Flavin mononucleotide, MB = methylene blue.

and electrochemical assay techniques. Indeed, NMR analysis of the cycled electrolytes detected no crossed over reactants and no evidence of decomposed BTMAP-Fc.

Developing new or tailored techniques capable of rationalizing full cell capacity fade in terms of specific mechanisms of molecular loss, particularly when the total capacity fade at the end of an experimental run at room temperature is ≤1%, is critical. It would greatly accelerate the assessment of novel strategies for molecular engineering of RFB chemistries with improved cell performance characteristics (e.g., open-circuit voltage, peak galvanic power density, and volumetric energy density) that still possess the long lifetimes required for commercialization. This need is illustrated by a recent study by DeBruler et al.[127] of a new RFB chemistry in which a sulfonate-functionalized viologen (1,1′-bis(3-sulfonatopropyl)-4,4′-bipyridinium, $(SPr)_2V$) and I^-/I_3^- were used in the negolyte and posolyte, respectively (Figure 5). This system features negatively charged redox-active moieties and cationic counterions—and thus potentially enables both higher maximum power densities and more durable RFBs than previous cationic MV/TEMPO or Fc configurations with anionic counterions—via the use of higher conductivity, longer-lifetime cation-exchange membranes.[131] The lowest apparent capacity fade rate attained for a negolyte-limited $(SPr)_2V$/KI cell was equivalent to 0.45%/day in galvanostatic cycling; however, with a cycling duration ∼2 days long, this amounts to a total capacity fade of only 1%, and NMR and CV analysis of cycled electrolytes failed to detect any decomposed or crossed over products. As a result, the promise of this potentially significant innovation is yet to be demonstrated or fully appreciated. Similar concerns apply to other advanced organic RFB concepts, such as those based on molecules comprising combined MV-Fc[132] or phenazine-TEMPO[119] moieties, differential pH MV-air systems,[133] hybrid metal−organic polymer configurations,[134−137] and iron coordination complexes with negolyte/posolyte redox potentials dictated by appropriate choice of ligand.[126]

Aza-aromatics, which contain nitrogen atoms in the aryl rings, have received attention as candidate RFB reactants.[34,79,138−143] More comprehensive assessments of capacity fade have the potential to accelerate the discovery and development of long-lived aza-aromatic chemistries. Quinoxaline, which comprises a fused benzene-pyrazine ring, was first proposed as a promising negolyte reactant by Milshtein et al.[138] owing to its high solubility (∼4.5 M in water, 0.5 M in 1 M KOH) and low reduction potential of −0.78 V vs SHE at pH 14. A subsequent patent application[144] reports quinoxaline full cells with BQDS and ferrocyanide posolytes that both exhibited rapid capacity decay, equivalent to greater than 100%/day. A proof-of-concept negolyte-limited quinoxaline/oxygen flow cell[142] exhibited a high apparent capacity fade rate as well, equivalent to ∼10%/day. However, this figure was not partitioned into contributions from molecular decomposition and crossover, the latter of which is expected to be moderately high for most charge-exclusion-based membranes, given that unsubstituted quinoxaline is uncharged.

Aza-aromatics with charged, hydrophilic side chains have demonstrated considerably lower capacity fade rates in full cells. This is the case for bioinspired, quinoxaline-like heterocycles, based in particular on phenazine[34] and phenothiazine (i.e., comprising either pyrazine or thiazine, respectively, sandwiched between two benzene rings), but also others based on alloxazine[79,139] (Table 3). Hollas et al.[34] synthesized dihydroxyphenazine sulfonic acid (DHPS) for use as a negolyte reactant in an alkaline flow cell, which has the best performance so far among aza-aromatic negolytes. At pH 14, DHPS has the lowest reduction potential of any organic negolyte species (−0.81 V vs SHE), a high solubility (1.8 M) and is essentially tied for the lowest apparent capacity fade rate among aza-aromatics in a cell

https://dx.doi.org/10.1021/acs.chemrev.9b00599
Chem. Rev. 2020, 120, 6467−6489

against a ferrocyanide posolyte (0.68%/day). Capacity loss was deemed unlikely to be accounted for by DHPS decomposition, given that an *ex situ* NMR study showed no decomposition of the oxidized form after 3 weeks of storage at pH 14; however, a similar study of the reduced form, which is more difficult due to the need to protect from oxidation by atmospheric O_2 invasion, was not performed. Visual inspection of the ion-exchange membrane after cycling showed intense discoloration, which led the authors to suggest that DHPS interaction with or crossover through the ion-exchange membrane was the more likely culprit. This hypothesis was supported by a concentration-independent temporal capacity fade rate, which is consistent with a mechanism for molecule loss with a first order dependence in concentration.

Replacing one of the nitrogen atoms in phenazine with a more electron-withdrawing sulfur atom yields phenothiazine, and Zhang et al. have recently shown that methylene blue (MB), an ammonium-functionalized phenothiazine, is a chemically stable derivative with a high enough redox potential under acidic conditions (0.57 V vs SHE) for use in the posolyte of a full cell.[145] DFT calculations suggested that the solvation of MB in acetic acid should be greater than in water. This enabled an ∼10× higher MB solubility in a mixture of acetic acid and sulfuric acid (1.8 M) than in water alone (<0.2 M). A full cell with an MB posolyte as the CLS and a negolyte based on the V^{2+}/V^{3+} redox couple displayed moderate apparent capacity fade rates of 0.52 and 0.76%/day for MB concentrations of 1.2 and 1.5 M, respectively. Similar to the case of phenazine, these fade rates were inconsistent with the apparently extremely high chemical stability of MB (established in this case by symmetric cell cycling, which we discuss in the next section); thus, capacity loss was attributed to continuous vanadium ion crossover through the anion-exchange membrane, resulting in the negolyte becoming the CLS. Based on these results and those of other studies involving pyridinic and phenazine-based reactants,[140,143] it appears that a wide variety of aza-aromatic molecules may be particularly promising for use in future RFBs, if their chemical stability can be more definitively established and compatible membranes and counter-electrolytes can be found.

Alloxazine-based alkaline full cells exhibit similar temporal capacity fade rates; however, molecular decay appears to play a more significant role than crossover. Lin et al.[79] and Orita et al.[139] reported cell chemistries with negolytes comprising, respectively, alloxazine 7/8-carboxylic acid (ACA), and flavin mononucleotide (FMN) mixed with nicotinamide (NA) to boost its water solubility. Both ACA and FMN derive from the isoalloxazine backbones of vitamin B_2, and the corresponding full cells with ferrocyanide posolytes exhibited temporal apparent capacity fade rates of 1.2 and 0.6%/day for negolyte reactant concentrations of 0.5 and 0.24 M, respectively. Lin et al. attributed capacity fade in ACA to OH^--initiated hydrolysis of the amidic carbonyls followed by a ring-opening reaction and further hydrolysis into redox-inactive species, which, as previously discussed, is a mechanism strongly supported by prior chemical studies[76−78,146] and an NMR study of the chemical stability of ACA in pH 14 solution.

Orita et al. conducted CV measurements of FMN in 1 M KOH at 363 K, and observed that a more irreversible redox couple ∼300 mV lower than that of FMN evolved and grew over the course of 100 h. Given that alloxazine hydrolysis products are not redox-active, and the new redox feature was present at pH 5.5 and 8.6, they concluded that the new CV features were unrelated to OH^--initiated hydrolysis products. Rather, they attributed the new CV peaks to the FMN dimer[147] which, they argued, should have a lower redox potential than the corresponding monomers owing to energetically favorable dipole−dipole interactions. This conclusion was supported in part by UV−vis absorption measurements that showed attenuated $\pi \rightarrow \pi^*$ transitions from FMN monomers over time. CVs of the cycled electrolyte failed to detect evidence for reactant crossover, indicating that molecular decomposition or diminution of redox activity is the main mechanism of active reactant loss. The relative contributions of irreversible FMN dimer formation and hydrolysis to capacity fade were not explored in detail; however, this finding of irreversible FMN dimerization raises the question of whether both mechanisms might be generally operative in alkaline alloxazine-based cells. There is some support for this notion from (i) CVs of ACA and charging profiles of ACA/$Fe(CN)_6$ full cells[79] displaying features similar to what was observed for FMN, and consistent with ACA dimer formation and (ii) the capacity fade rate for the ACA/$Fe(CN)_6$ cell being twice that of FMN/$Fe(CN)_6$, for a concentration of ACA that is twice that of FMN − this is consistent with capacity fade originating from a mixture of first order (OH^--initiated hydrolysis) and second-order (dimerization) decay mechanisms.

2.3. Symmetric Cell Cycling: A Technique for Coupling Capacity Fade to Chemical Decomposition

In full cells, both CLS active reactant chemical decomposition and crossover across the membrane[37,88] contribute to capacity fade. Thus, where reactant permeability is non-negligible, quantifying the role of molecular decomposition alone to cell capacity fade is difficult. One potentially simple way of decoupling molecular decomposition from crossover is by using a cell in which both the negolyte and posolyte have the same redox couple at the same concentration; this way, reactant diffusion through the membrane is virtually eliminated because of similar chemical compositions on either side of it. Darling and Perry[148] implemented the first embodiment of this idea in the form of a "double half-cell" configuration in which a 50% SOC V^{2+}/V^{3+} electrolyte from a single reservoir was circulated across a cell stack that was held at a constant potential such that electrolyte oxidation occurred at one electrode and reduction at the other. In principle, if there are no side reactions, an open-circuit potential of 0 V and constant SOC would be maintained in the reservoir, diffusion-induced reactant and solvent crossover would be eliminated, and the measured current would be proportional to the concentration of vanadium ions. Although this technique is useful for evaluating the performance of a cell stack, one could not use the measured current as a proxy for reactant concentration because it would be sensitive to changes in membrane resistance, electron-transfer kinetics and ambient temperature, in addition to concentration changes from molecular decomposition.

A route to avoiding these limitations is the symmetric cell configuration, in which two separate electrolyte reservoirs contain the same redox couple (Figure 6a), and their Coulombic capacity is measured with constant-current (Figure 6b) or constant-voltage cycling. This approach, first reported by Milshtein et al.[149,150] for nonaqueous RFB chemistries, enables the assessment of capacity fade because, in the absence of significant mass transport overpotentials, capacity is directly related to reactant concentration. Goulet and Aziz[33] presented a variation called the "unbalanced, compositionally symmetric cell

https://dx.doi.org/10.1021/acs.chemrev.9b00599
Chem. Rev. 2020, 120, 6467−6489

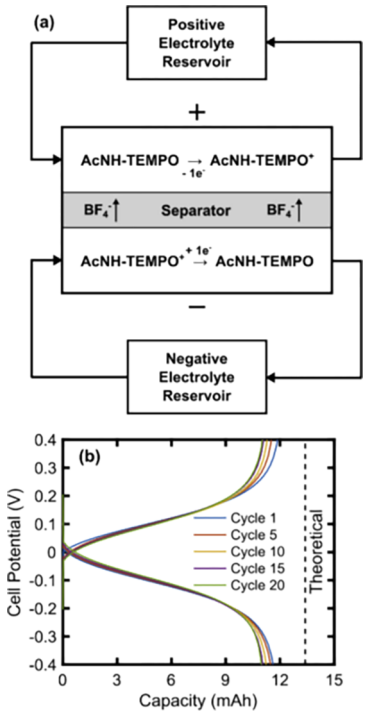

Figure 6. (a) Schematic of a symmetric flow cell during charging of a TEMPO-based molecule in nonaqueous electrolyte. (b) Potential vs charge for selected cycles of symmetric cell cycling of 50 mM total active species in 0.5 M $LiBF_4$/PC. Reprinted with permission from ref 149. Copyright 2016 Elsevier.

method", in which the electrolytes were compositionally symmetric but volumetrically unbalanced, so that one side is the CLS during both charge and discharge, and the other the NCLS (Figure 7a). By implementing constant-potential cycling with this setup (Figure 7b), they demonstrated that the temporal capacity fade rate of the CLS correlates quantitatively with chemical instability of the redox couple contained therein. They also demonstrated that introducing pauses in cell cycling at different SOC values of the CLS could establish relative susceptibilities of the different redox states of the molecule of interest to chemical decomposition (Figure 7c). Symmetric-cell cycling is therefore a robust but simple means of evaluating molecular decomposition rates and of informing molecular engineering strategies for developing long-lived aqueous RFB reactants.

Symmetric cell cycling is relatively rare in the molecular RFB literature, but it has shed light on chemical stability of and cell results particularly involving quinone,[33,53,54,61,100,151] viologen,[33] aza-aromatic,[145] ferrocyanide,[33,56,64] and TEMPO-based[118] molecules (Table 4). The single-electrolyte capacity fade rate revealed by these measurements is expected to provide a lower limit on the fade rate of a full cell pairing that electrolyte against another electrolyte. We have found only two exceptions in the literature[54,100] and can hypothesize an explanation in one case: Ji et al.[54] performed symmetric-cell cycling at a different pH than the full-cell cycling reported in the same work. An extremely low (0.02%/day and lower) full cell capacity fade rate has been established for 2,6-DPPEAQ/$K_4Fe(CN)_6$,[54] demonstrating that organic molecules can possess the lifetime properties necessary for RFB commercialization. Comparably low apparent fade rates of other species offer the possibility of more such demonstrations.[56,145,152] Where temporal fade rates are moderate (0.1−1%/day) or worse, symmetric cell cycling is a particularly powerful diagnostic tool. The lowest reported full cell apparent fade rate for AQDS, for instance, is 0.2%/day for a concentration of 0.5 M,[153] which is reasonably consistent with the symmetric cell fade rate of 0.08 ± 0.02%/day obtained in potentiostatic cycling for a concentration of 0.1 M.[33] Pausing the symmetric cell at 100% SOC resulted in capacity loss equivalent to 0.2%/day, whereas a similar hold at 0% SOC resulted in no

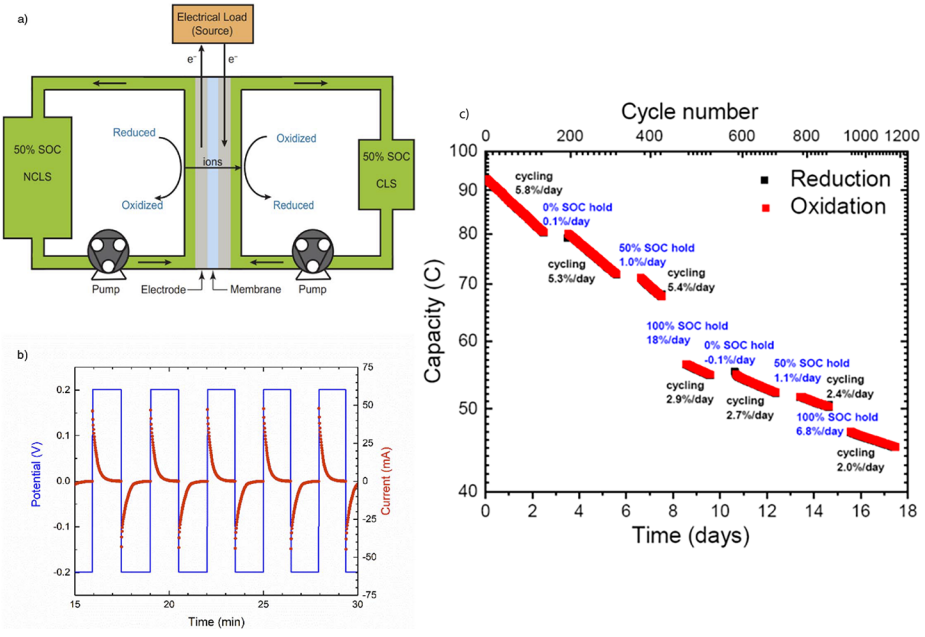

Figure 7. (a) Schematic of unbalanced, compositionally symmetric flow cell. (b) Example of symmetric cell potentiostatic cycling protocol. (c) Semilog plot of unbalanced, compositionally symmetric cell cycling of 50% SOC 0.1 M DHAQ in 1 M KOH with cycling pauses at different SOCs. Temporal capacity fade rates from slopes of each cycling segment are denoted in black text. Capacity loss and SOC of CLS during 24-h pauses are denoted in blue text. Reprinted with permission from ref 33. Copyright 2018 Electrochemical Society.

https://dx.doi.org/10.1021/acs.chemrev.9b00599
Chem. Rev. 2020, 120, 6467−6489

Table 4. Summary of Symmetric Cell Results, Arranged by Class of Molecule[a]

name	author/year	capacity fade rate		electron conc. (M)	redox potential (V vs SHE)	pH
		%/cycle	%/day			
quinones						
DHAQ	Goulet/2018[33]	**0.14**	**6**	0.2	−0.68	14
2,3-HCNQ	Wang/2018[100]	0.12	7.3	0.2	−0.53	14
2,6-DBEAQ	Kwabi and Lin/2018[53]	**0.001**	**0.008**	0.2	−0.52	14
		0.001	**0.0075**	1.3	−0.52	14
		0.0002	**0.007**	0.2	−0.52	12
2,6-DPPEAQ	Ji/2019[54]	0.00035	0.02	0.2	−0.47	13
AQDS	Goulet/2018[33]	**0.001**	**0.08**	0.2	0.20	0
DHDMBS	Murali/2018[61]	0.03	0.48	1.1	0.85	0
TMHQ	Drazevic/2019[151]	0.7	70	0.05	0.89	7
viologens						
BTMAP-Vi	Goulet/2018[33]	**0.000014**	**0.0016**	0.1	−0.36	7
Methyl-Vi		**0.015**	**1.5**	0.1	−0.45	7
aza-aromatics						
MB	Zhang/2019[145]	0.00077	0.016	2	0.57	−0.5
iron coordination complexes						
$K_4Fe(CN)_6$	Goulet/2018[33]		**8**	0.1	0.50	14
	Luo/2017[64]	0.24	21	0.2	0.50	14
		0.026	2.3	0.2	N/A	10
		0.008	0.7	0.2	0.39	7.2
$(NH_4)_4Fe(CN)_6$	Luo/2018[56]	0.00027	0.017	0.5	0.39	7
nitroxide radicals						
TMAP-TEMPO	Liu/2019[118]	**0.0076**	**0.55**	0.1	0.81	7

[a]Capacity fade results established by potentiostatic cycling or galvanostatic cycling with potentiostatic finishes are marked in bold text, whereas purely galvanostatic results for apparent capacity fade are left in plain text. "electron conc." refers to moles of transferrable electrons per liter of electrolyte. TMHQ = tetramorpholinohydroquinone.

perceptible change in capacity, leading to the conclusion that the reduced form of AQDS is more susceptible to decomposition than the oxidized form. This conclusion is corroborated by an NMR study showing a 40% reduction in AQDS concentration after 2 weeks of storage at 45 °C in the reduced form, while the oxidized form stayed intact under identical treatment. Regarding DHAQ, combinations of full and symmetric cell experiments together with NMR and HPLC analysis[32,33] have shown both that the 5−8%/day fade rate observed in full cell cycling is quantitatively attributable to chemical decomposition and that the disproportionation of reduced DHAQ to its corresponding quinone and anthrone forms, and the dimerization of the latter is the capacity-loss mechanism.

It remains an intriguing open question whether symmetric cell cycling combined with chemical analysis can discern the link between capacity fade and molecular decomposition in other molecules and molecule classes. For instance, although Tong et al. provided evidence that tautomerization was the main mode of bislawsone decomposition,[98] they did so with a full rather than symmetric cell, and about 46% of the cell's capacity loss could not be accounted for by chemical decomposition. Wang et al.,[100] on the other hand, showed that a 2-hydroxy-3-carboxy-1,4-naphthoquinone (2,3-HCNQ) symmetric cell loses capacity faster at 100% SOC (13.4%/day) than 0% SOC (0.6%/day) but did not perform follow-up chemical analysis, and thus did not verify that tautomerization of the reduced form was the main capacity-loss mechanism. Symmetric cell cycling has been employed in attempting to elucidate the proto-desulfonation reaction in DHDMBS,[61] the dimerization and protonation of reduced MV and BTMAP-Vi, respectively,[33] and nucleophilic attack by water in TEMPO-based chemistries.[118] In principle, it can be applied to great effect to precisely elucidate the kinetics and sensitivity to SOC of these and other hypothesized decay mechanisms, such as dimerization and hydrolysis of alloxazines,[79,139,147] and gem-diol formation and nucleophilic Michael reactions in quinones.[59]

As with full cell cycling, however, deploying the appropriate symmetric cell cycling protocol is critical if one intends to ensure that measured capacities most closely reflect actual amounts of active reactants. First, the two electrolytes should ideally not be capacity-balanced, in order that only one electrolyte (the CLS) experiences the excursions in SOC prescribed during electrochemical cycling. This permits direct attribution of capacity fade measured at the cell level to a single electrolyte without the need for further partitioning, and eases *ex situ* chemical analysis because, under ideal circumstances, decomposition of molecules in the NCLS will not contribute to capacity fade. Second, cycling with potential holds to access the maximum capacity (i.e., either potentiostatic, or galvanostatic with potential hold finishes) is more accurate than purely galvanostatic cycling, as the latter is vulnerable to spurious changes in apparent capacity caused by temporal changes in mass transport, ambient temperature fluctuations, and drifts in membrane resistance and electrode kinetics.[33,90] Caution must be exercised in interpreting results obtained under such circumstances. Indeed, extremely low apparent capacity fade in purely galvanostatic symmetric cell cycling tests[56,145] may be the result of a fortuitous combination of progressively lower cell resistance and significant actual capacity loss, rather than high chemical stability of the redox couple in question.

Capacity retention results from hybrid full-symmetric cells, in which the two electrolytes are identical, each comprising both high and low-potential redox couples,[56] cannot necessarily be interpreted directly in terms of reactant stability. Much like a full

https://dx.doi.org/10.1021/acs.chemrev.9b00599
Chem. Rev. 2020, 120, 6467−6489

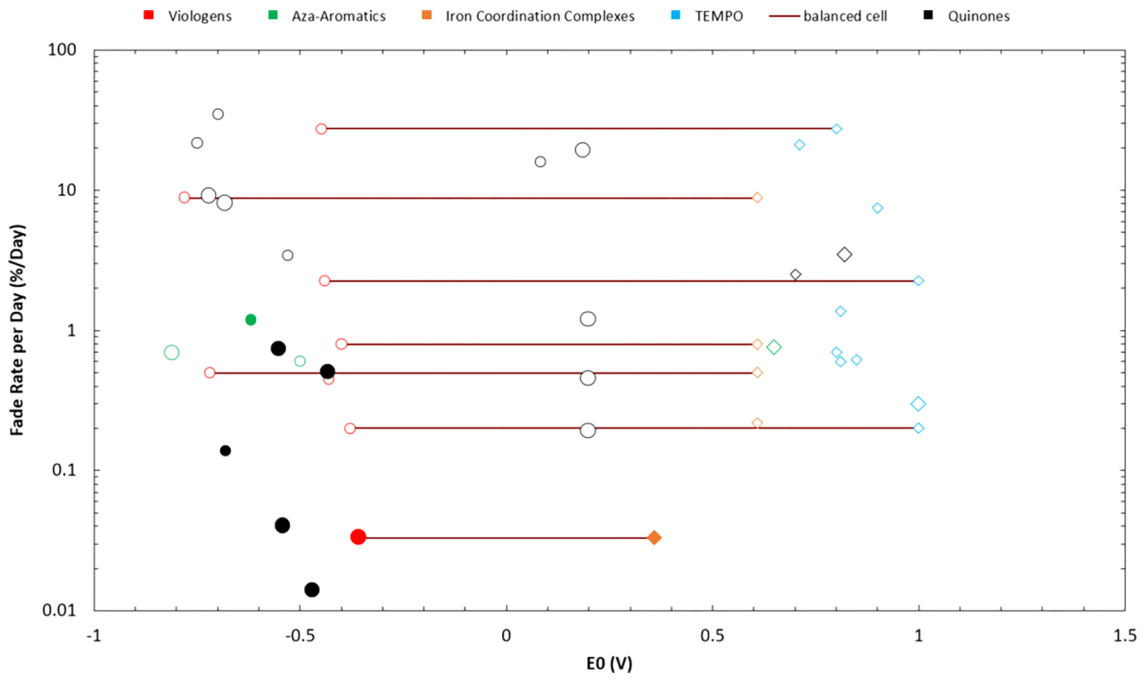

Figure 8. Plot showing full cell capacity fade rate in%/day vs redox potential (vs SHE) for viologen (red), aza-aromatic (green), iron coordination complex (orange), TEMPO (blue), and quinone-based (black) chemistries. Posolytes are indicated using diamonds, and negolytes in circles, whereas points depicting chemistries with electron concentrations ≥1.0 M are larger than those <1.0 M. Points depicting capacity fade results of chemistries that have been tested using potentiostatic or combined potentiostatic-galvanostatic cycling have been filled, whereas those depicting apparent capacity fade results obtained with only galvanostatic cycling have been left empty. Capacity-balanced cells where both sides contain organics/organometallics are marked out with a horizontal line connecting negolyte and posolyte chemistries.

cell, this method features a nonzero average cell potential during charge/discharge. One oxidizes/reduces the high-potential redox couple in one electrolyte while reducing/oxidizing the low-potential couple in the other, with the complementary redox couples acting as "dormant" spectators. Low apparent capacity fade rates in this case are not sufficient to establish high chemical stability of the redox couples involved because at low or high SOC values there could be asymmetric crossover[33] of dormant material, in such a way as to compensate for decomposed species in the side that is or becomes capacity-limiting; this replenishment would mask the actual capacity fade. Additionally, capacity fade could comprise fractional decomposition among four redox species, each of which is experiencing potential oscillations over two distinct ranges, making useful interpretation difficult. This is particularly exacerbated when the cell polarity is switched after a number of cycles and previously dormant active material is accessed electrochemically. Luo et al.[56] argued that switching the polarity midway through a cycling regimen demonstrates that species have not been lost through crossover; however, extremely small errors in exactly balancing the original volumes on the two sides could vitiate this argument.

In cases where there are deleterious interactions between the electrolyte-contacting materials and redox-active molecules, symmetric cell cycling may yield an artificially high capacity fade rate that underestimates the actual chemical stability of the redox couple under consideration. This is the case for cycling of the ferro-/ferricyanide redox couple on activated carbon paper electrodes at high pH,[33] and may also apply to tetramorpholinoquinone (TMHQ).[151] In the case of unbalanced compositionally symmetric cell cycling of $Fe(CN)_6$ at pH 14, Goulet and Aziz observed an acceleration in the instantaneous capacity fade rate, from <10%/day up to 45−67%/day.[33] UV−vis and CV measurements jointly established that contact between ferricyanide solution at pH 14 and the carbon electrode even under open-circuit conditions resulted in the spontaneous reduction of the former to ferrocyanide. This had the effect of making both electrolytes capacity-limiting after the passage of enough time in the symmetric cell. The precise mechanistic details of ferricyanide reduction are yet to be understood, however there is evidence that it occurs faster with increasing concentration of OH^- and light exposure. Given that both the concentration of OH^- and light exposure have been implicated in accelerating the replacement of the cyanide ligand in $Fe(CN)_6$ with hydroxl,[64,154,155] determining the interplay between these two mechanisms and their relative contributions to capacity fade is critical. Understanding the implications of this interplay is particularly urgent for full cell cycling, because most posolytes in alkaline organic flow cells comprise the $Fe(CN)_6^{3-/4-}$ redox couple (see Table 1). Drazevic et al.[151] speculated that a similar carbon-mediated reduction mechanism may be at play in symmetric cell cycling of TMHQ, based on the observation that *ex situ* LC-MS analysis of cycled electrolytes cannot rationalize total capacity fade in terms of irreversible tautomerization and hydrolysis of oxidized TMHQ. Future aqueous organic RFB research should therefore focus on the development of methods that can comprehensively map out the landscape of chemical and electrochemical decomposition in these more complex chemistries.

It is important to note that, in practical deployment, RFBs will operate on variable power-based profiles rather than cyclic galvanostatic/potentiostatic profiles in which the average SOC of the CLS is close to 50%. Consequently, understanding how capacity fade in a flow cell varies with SOC by introducing pauses at different SOC values[33] or restricting the SOC range experienced by the CLS[32] may be useful starting points in predicting RFB longevity in real-world applications. In any case,

https://dx.doi.org/10.1021/acs.chemrev.9b00599
Chem. Rev. 2020, 120, 6467−6489

translating capacity fade measured at the laboratory-scale to a practical RFB is a complex undertaking, and will require further study as load profile standards for grid-scale storage devices are adopted.

3. SUMMARY

We list and elaborate upon key findings of this review below:

- As shown in Figure 8, which shows the full cell capacity fade rate vs redox potential for chemistries reported in Tables 1−3, quinone and viologen-based chemistries are the most studied for use in aqueous organic negolytes, and full cells featuring them as the CLS exhibit a wide range of fade rates. In most cases, capacity fade results in large part from chemical decomposition of active reactants, the mitigation of which through synthetic modification has received intense research attention.
- For viologens, functionalization with charged ammonium groups considerably slows down viologen dimerization, enabling a low capacity fade rate in the case of a BTMAP-Vi/BTMAP-Fc cell. Quinones are susceptible to a large number of decay mechanisms (nucleophilic addition/substitution, disproportionation, dimerization, and tautomerization); however, oxy-alkyl substitutions, as in 2,6-DPPEAQ and 2,6-DBEAQ, appear to suppress tautomerization and disproportionation under alkaline conditions, and afford the only currently demonstrated pathway to extremely low fade rates in full cells.
- Negolytes based on aza-aromatic molecules have received less attention, but are potentially promising RFB reactants in terms of chemical stability. Capacity fade in phenazine and phenothiazine-based full cells appears to originate in large part from crossover and membrane incompatibility issues; however, independent assessments of reactant chemical stability have not been thorough enough to establish this conclusion.
- Aqueous organic or organometallic posolyte development lags far behind negolyte development: only one capacity-limiting organic posolyte, BTMAP-Fc,[90] which has a relatively low redox potential, has demonstrated a low temporal capacity fade rate (less than 0.1%/day). In the case of quinones, this observation is consistent with theoretical calculations suggesting that quinones with reduction potentials greater than 0.9 V vs SHE are highly susceptible to irreversible nucleophilic attack by water. For acidic negolyte chemistries, the inorganic bromine/bromide redox couple is thus frequently used in the posolyte, whereas $Fe(CN)_6^{3-/4-}$ is nearly ubiquitous against organic negolytes in alkaline conditions.
- TEMPO derivatives, used most frequently in neutral pH, generally exhibit moderate-to-high fade rates in full cells, presumably owing to nucleophilic attack by water. In contrast to Fc, functionalization with ammonium groups[118,121] does not drastically reduce fade rates to low or extremely low levels. Both of these statements are consistent with a recent report[118] demonstrating that the temporal fade rate of flow cells containing an ammonium-functionalized TEMPO derivative is independent of concentration (see Table 2).
- Combining electrochemical full cell cycling with *ex situ* chemical analysis of cycled electrolytes has been a common means of illuminating the relationship between capacity fade and chemical decomposition. Whereas this technique has been successful for cell chemistries that lose capacity at >0.1%/day, it is limited in doing the same for longer lasting chemistries because, for more stable chemistries, it becomes increasingly difficult to run experiments for sufficient durations to reach the sensitivity limits of most chemical analysis tools.
- As shown in Tables 1−3, there is a poor correlation between time- and cycle-denominated capacity fade rates. We therefore expect the cycle-denominated capacity fade rate to be a poor predictor of RFB reactant chemical lifetime under conditions of practical deployment unless proven otherwise.
- A significant number of chemical stability studies of proposed RFB reactant are conducted using galvanostatic cycling, which is inadequate for quantifying low or extremely low fade rates due to possible artifacts introduced by temporal changes in mass transport, ambient temperature fluctuations, and drifts in membrane resistance or electrode kinetics. Far more reliable for this purpose are potentiostatic cycling or galvanostatic cycling with potential holds at the end of charging and of discharging of every n th cycle, where only the capacities measured potentiostatically are taken seriously.
- A technique that more tightly couples capacity fade to chemical decomposition is potentiostatic cycling of volumetrically unbalanced, compositionally symmetric cells, along with holds at various SOC to evaluate temporal fade rate vs SOC. It has been used to elucidate decomposition mechanisms in a number of quinone-based chemistries[32,33,98,151] and should be extended to other molecular classes.

4. CONCLUSIONS

The potentially long discharge duration at rated power that is attainable with RFBs makes them promising for surpassing lithium ion batteries for safe, low-cost, large-scale storage for discharge durations of several hours or longer. Aqueous organic RFBs have potentially lower cost than their vanadium-based counterparts; however, this depends on finding negolyte and posolyte chemistries that achieve low levelized cost through a combination of long chemical and crossover lifetime, low synthetic cost at scale, and adequate safety, energy density, and power density. Because there is a reasonably well-known floor to the mass-production cost of organic chemicals, attaining and demonstrating long chemical lifetime is the greatest present challenge for aqueous organic RFBs.

A significant amount of research attention needs to be paid to understanding the mechanisms responsible for capacity fade, as a basis for rational engineering of robust RFBs. Understanding chemical decomposition, in particular, is important because organic and organometallic redox couples tend to be less stable than purely inorganic ones. This task is challenging, because the main molecules are susceptible to several decomposition mechanisms in water that incur loss or diminution of redox activity, such as nucleophilic reactions, disproportionation, dimerization and tautomerization. In flow cells, these pathways may be simultaneously operative, with overlapping time scales and unknown rates and reaction orders.

Based on our survey of the literature, we surmise the following:

- For all aqueous organic electrolytes for which we have observed sufficient experimentation to distinguish

https://dx.doi.org/10.1021/acs.chemrev.9b00599
Chem. Rev. 2020, 120, 6467−6489

between cycle-denominated fade and time-denominated fade, it has been found that the amount of lost capacity is essentially independent of the number of charge−discharge cycles to which a species is subjected. Rather, capacity fade is primarily time-denominated. The temporal fade rate can depend on molecular concentrations, pH and SOC. Thus, the capacity fade for new electrolytes should be presumed to be primarily time-denominated unless a cycle-denominated component is proven to be significant.

- Irreversible capacity fade can arise from reactant crossover or decomposition, or electrolyte leakage. Apparent capacity fade that is recoverable, which can arise from a variety of other effects such as a side reaction putting the two sides out of balance, can prevent direct attribution of apparent capacity fade measured at the cell level to these irreversible capacity fade mechanisms.
- Definitively establishing molecular decomposition rates less than about 0.1%/day requires careful experimentation and simple experimental designs in which interference from competing effects such as crossover are suppressed. Results are more convincing if close correlation of capacity fade to chemical decomposition is established by chemical analysis, but this becomes increasingly difficult with lower fade rates. Symmetric-cell cycling can be interpreted more readily than full-cell cycling due to the suppression of contamination issues associated with reactant crossover. Volumetrically unbalanced compositionally symmetric cell cycling (Figure 7) is recommended because the fade rate can be attributed to the SOC of only the CLS.
- Inferences about molecular decomposition mechanisms can be made by holding both oxidized and reduced forms of reactants in the presence or absence of electrolyte-contacting materials, or at various pH values, durations and temperatures, followed by chemical analysis using such techniques as cyclic voltammetry, NMR, and mass spectrometry. Accelerated *ex situ* chemical decomposition at elevated temperatures may permit elucidation of slower capacity fade rates at lower operating temperatures, but this is valid only if the dominant degradation mechanism does not change within the chosen temperature range.
- The vast majority of aqueous-soluble redox-active organic and organometallic compounds reported to date have high (>1%/day) or moderate (0.1−1%/day) fade rates (see Tables 1−4), which are too high for RFB project lifetimes anticipated to last decades. Only a few have low (0.02−0.1%/day) fade rates, and very few (2,6-DPPEAQ, 2,6-DBEAQ, BTMAP-Fc, BTMAP-Vi, $(NH_4)_4Fe(CN)_6$ and MB) have extremely low (≤0.02%/day) established or apparent capacity fade rates. Only 2,6-DPPEAQ, 2,6-DBEAQ, BTMAP-Vi, and BTMAP-Fc have had their fade rates established by potentiostatic cycling. Some of these (2,6-DPPEAQ, 2,6-DBEAQ, and BTMAP-Vi) have been established in symmetric-cell cycling and two (2,6-DPPEAQ and BTMAP-Fc) have been established as the CLS in full-cell cycling.
- Posolyte development deserves increased attention. No posolyte-limited full cell configurations with an open-circuit voltage greater than or equal to 1.0 V and a temporal fade rate less than 0.1%/day have been reported. The only full cells with open-circuit voltages ≥1.0 V with "low" or "extremely low" fade rates are 2,6-DBEAQ/$Fe(CN)_6$ and 2,6-DPPEAQ/$Fe(CN)_6$, both of which were negolyte-limited. $K_4Fe(CN)_6$ is challenging as an RFB posolyte because it has limited solubility (~0.8 M at pH 7[56,156] and lower at higher pH), its crossover and chemical decomposition rates can be significant, and its mass-production cost, though well below that of vanadium, is a concern. Bromine is likewise problematic as an acidic posolyte because it has a high crossover rate and high cost of safe containment. This highlights the need for further investigation into low-cost, high-potential redox couples possessing high chemical stability.
- Because increasing reactant concentration reduces the levelized cost of RFB storage for a given chemistry, research into highly soluble organics is important. All full-cell chemistries for which low or extremely low capacity fade rates have been established have featured CLS reactant concentrations equivalent to ≥1 M of transferrable electrons. Other chemistries have this attribute but exhibit moderate fade rates (AQDS, DHPS, PEGAQ, bislawsone, and MB).

AUTHOR INFORMATION

Corresponding Author

Michael J. Aziz − *Harvard School of Engineering and Applied Sciences, Cambridge, Massachusetts 02138, United States;* orcid.org/0000-0001-9657-9456; Email: maziz@harvard.edu

Authors

David G. Kwabi − *Department of Mechanical Engineering, University of Michigan, Ann Arbor, Michigan 48109, United States;* orcid.org/0000-0003-3663-8789

Yunlong Ji − *Department of Chemistry and Chemical Biology, Harvard University, Cambridge, Massachusetts 02138, United States;* orcid.org/0000-0002-1124-4209

Complete contact information is available at: https://pubs.acs.org/10.1021/acs.chemrev.9b00599

Notes

The authors declare no competing financial interest.

Biographies

David G. Kwabi obtained a B.S.E in Mechanical Engineering and a certificate in Materials Science and Engineering at Princeton University in 2010. He carried out M.S. and Ph.D. studies in Mechanical Engineering at the Massachusetts Institute of Technology from 2010 until 2016, under the supervision of Prof. Yang Shao-Horn, in the field of Li−O_2 batteries. He subsequently joined the group of Prof. Michael J. Aziz at Harvard University as a postdoctoral scholar, where he worked on aqueous organic redox-flow batteries. In January 2019, he joined the Mechanical Engineering department at the University of Michigan as an assistant professor. His research is in the investigation of fundamental reaction mechanisms and morphological transformations in advanced electrochemical energy storage systems such as conversion and flow batteries.

Yunlong Ji obtained his B.A. degree in Chemistry from Central South University in 2010. He then pursued his graduate studies in organic synthesis and fluorine chemistry at Shanghai Institute of Organic Chemistry, Chinese Academy of Sciences under the supervision of Prof. Jichang Xiao. In 2015, he started his postdoctoral research in organic semiconductor materials with Prof. Jian Li at Arizona State University.

https://dx.doi.org/10.1021/acs.chemrev.9b00599
Chem. Rev. 2020, 120, 6467−6489

He was a postdoctoral associate with Professor Roy G. Gordon and Professor Michael J. Aziz at Harvard University from 2017 to 2019, where his work focused on aqueous organic redox flow batteries. He received his faculty position at Zhejiang Sci-Tech University and began his independent career in January 2020. His research interests include the design, synthesis, and characterization of organic materials for energy storage and conversion applications.

Michael J. Aziz received a B.S. from Caltech in 1978 and a Ph.D. in Applied Physics from Harvard in 1983. He spent two years at Oak Ridge National Laboratory as Eugene P. Wigner Postdoctoral Fellow. He has been a member of the faculty at what is now the Harvard John A. Paulson School of Engineering and Applied Sciences since he joined in 1986 and is now Gene and Tracy Sykes Professor of Materials and Energy Technologies. He has made significant contributions to a number of fields in applied physics and materials science including the kinetics of rapid solidification, pressure and stress effects on kinetics of diffusion and growth, nonequilibrium surface pattern formation during ion irradiation, and applications of materials synthesized utilizing nonequilibrium kinetics. His recent interests involve energy storage and CO_2 capture. He has directed a multi-investigator research program on stationary electrical energy storage since 2012 and is coinventor of the aqueous organic redox flow battery, with multiple patents that have been licensed for commercialization. He is corecipient of the 2019 Energy Frontiers Prize from Eni for these developments. He served as the Faculty Coordinator for Harvard's University-Wide Graduate Consortium on Energy and Environment from 2009 to 2018, for which he developed a quantitative course on Energy Technology for a group of students in diverse disciplines, and is currently authoring a textbook on energy technology.

ACKNOWLEDGMENTS

Research at Harvard has been supported by U.S. DOE Award DE-AC05-76RL01830 through PNNL Subcontract 428977, by U.S. DOE ARPA-E Award DE-AR-0000767, by Innovation Fund Denmark via the Grand Solutions project "ORBATS" file No. 7046-00018B, by the U.S. National Science Foundation through Grant No. NSF CBET-1914543, and by the Massachusetts Clean Energy Technology Center. We thank Sanat Modak and Swayam Patnaik for assistance in compiling and plotting the results from the literature and Eric Fell and Dr. Yan Jing for helpful discussions.

REFERENCES

(1) IPCC *Climate Change 2014: Synthesis Report*; IPCC, 2014.
(2) Raupach, M. R.; Marland, G.; Ciais, P.; Le Quere, C.; Canadell, J. G.; Klepper, G.; Field, C. B. Global and regional drivers of accelerating CO2 emissions. *Proc. Natl. Acad. Sci. U. S. A.* **2007**, *104*, 10288−10293.
(3) Pacala, S.; Socolow, R. Stabilization Wedges: Solving the Climate Problem for the Next 50 Years with Current Technologies. *Science* **2004**, *305*, 968−971.
(4) Ferrara, M.; Chiang, Y. M.; Deutch, J. M. Demonstrating Near-Carbon-Free Electricity Generation from Renewables and Storage. *Joule* **2019**, *3*, 2585−2588.
(5) Ziegler, M. S.; Mueller, J. M.; Pereira, G. D.; Song, J.; Ferrara, M.; Chiang, Y.-M.; Trancik, J. E. Storage Requirements and Costs of Shaping Renewable Energy Toward Grid Decarbonization. *Joule* **2019**, *3*, 2134−2153.
(6) Olivetti, E. A.; Ceder, G.; Gaustad, G. G.; Fu, X. Lithium-Ion Battery Supply Chain Considerations: Analysis of Potential Bottlenecks in Critical Metals. *Joule* **2017**, *1*, 229−243.
(7) Lisbona, D.; Snee, T. A review of hazards associated with primary lithium and lithium-ion batteries. *Process Saf. Environ. Prot.* **2011**, *89*, 434−442.
(8) Wang, Q.; Ping, P.; Zhao, X.; Chu, G.; Sun, J.; Chen, C. Thermal runaway caused fire and explosion of lithium ion battery. *J. Power Sources* **2012**, *208*, 210−224.
(9) Li, Z.; Pan, M. S.; Su, L.; Tsai, P.-C.; Badel, A. F.; Valle, J. M.; Eiler, S. L.; Xiang, K.; Brushett, F. R.; Chiang, Y.-M. Air-Breathing Aqueous Sulfur Flow Battery for Ultralow-Cost Long-Duration Electrical Storage. *Joule* **2017**, *1*, 306−327.
(10) Darling, R. M.; Gallagher, K. G.; Kowalski, J. A.; Ha, S.; Brushett, F. R. Pathways to low-cost electrochemical energy storage: a comparison of aqueous and nonaqueous flow batteries. *Energy Environ. Sci.* **2014**, *7*, 3459−3477.
(11) Lin, K.; Chen, Q.; Gerhardt, M. R.; Tong, L.; Kim, S. B.; Eisenach, L.; Valle, A. W.; Hardee, D.; Gordon, R. G.; Aziz, M. J.; Marshak, M. P. Alkaline quinone flow battery. *Science* **2015**, *349*, 1529−1532.
(12) Skyllas-Kazacos, M.; Chakrabarti, M. H.; Hajimolana, S. A.; Mjalli, F. S.; Saleem, M. Progress in Flow Battery Research and Development. *J. Electrochem. Soc.* **2011**, *158*, R55−R79.
(13) Skyllas-Kazacos, M.; Kazacos, G.; Poon, G.; Verseema, H. Recent advances with UNSW vanadium-based redox flow batteries. *Int. J. Energy Res.* **2010**, *34*, 182−189.
(14) Skyllas-Kazacos, M.; Kasherman, D.; Hong, D.R.; Kazacos, M. Characteristics and performance of 1 kW UNSW vanadium redox battery. *J. Power Sources* **1991**, *35*, 399−404.
(15) Moseley, P. T.; Garche, J. *Electrochemical Energy Storage for Renewable Sources and Grid Balancing*, 1st ed.; Elsevier: Amsterdam, 2014.
(16) Soloveichik, G. L. Flow Batteries: Current Status and Trends. *Chem. Rev.* **2015**, *115*, 11533−11558.
(17) Kreutzer, H.; Yarlagadda, V.; Van Nguyen, T. Performance Evaluation of a Regenerative Hydrogen-Bromine Fuel Cell. *J. Electrochem. Soc.* **2012**, *159*, F331−F337.
(18) Braff, W. A.; Bazant, M. Z.; Buie, C. R. Membrane-less hydrogen bromine flow battery. *Nat. Commun.* **2013**, *4*, 2346.
(19) Andrews, J.; Seif Mohammadi, S. Towards a 'proton flow battery: Investigation of a reversible PEM fuel cell with integrated metal-hydride hydrogen storage. *Int. J. Hydrogen Energy* **2014**, *39*, 1740−1751.
(20) Savinell, R. F.; Wainright, J. S. Iron flow batteries. U.S. Patent 9,559,375, 2017.
(21) Petek, T. J.; Hoyt, N. C.; Savinell, R. F.; Wainright, J. S. Slurry electrodes for iron plating in an all-iron flow battery. *J. Power Sources* **2015**, *294*, 620−626.
(22) Tucker, M. C.; Phillips, A.; Weber, A. Z. All-Iron Redox Flow Battery Tailored for Off-Grid Portable Applications. *ChemSusChem* **2015**, *8*, 3996−4004.
(23) Rajarathnam, G. P.; Vassallo, A. M. *The Zinc/Bromine Flow Battery: Materials Challenges and Practical Solutions for Technology Advancement*; Springer: Singapore, 2016.
(24) Li, B.; Nie, Z.; Vijayakumar, M.; Li, G.; Liu, J.; Sprenkle, V.; Wang, W. Ambipolar zinc-polyiodide electrolyte for a high-energy density aqueous redox flow battery. *Nat. Commun.* **2015**, *6*, 6303.
(25) Weng, G.-M.; Li, Z.; Cong, G.; Zhou, Y.; Lu, Y.-C. Unlocking the capacity of iodide for high-energy-density zinc/polyiodide and lithium/polyiodide redox flow batteries. *Energy Environ. Sci.* **2017**, *10*, 735−741.
(26) Gong, K.; Ma, X.; Conforti, K. M.; Kuttler, K. J.; Grunewald, J. B.; Yeager, K. L.; Bazant, M. Z.; Gu, S.; Yan, Y. A zinc-iron redox-flow battery under $100 per kWh of system capital cost. *Energy Environ. Sci.* **2015**, *8*, 2941−2945.
(27) Leung, P. K.; Ponce-de-León, C.; Low, C. T. J.; Shah, A. A.; Walsh, F. C. Characterization of a zinc-cerium flow battery. *J. Power Sources* **2011**, *196*, 5174−5185.
(28) Chen, H.; Cong, G.; Lu, Y.-C. Recent progress in organic redox flow batteries: Active materials, electrolytes and membranes. *J. Energy Chem.* **2018**, *27*, 1304−1325.
(29) Park, M.; Ryu, J.; Wang, W.; Cho, J. Material design and engineering of next-generation flow-battery technologies. *Nat. Rev. Mater.* **2017**, *2*, 16080.
(30) Hendriks, K. H.; Robinson, S. G.; Braten, M. N.; Sevov, C. S.; Helms, B. A.; Sigman, M. S.; Minteer, S. D.; Sanford, M. S. High-

https://dx.doi.org/10.1021/acs.chemrev.9b00599
Chem. Rev. 2020, 120, 6467−6489

Performance Oligomeric Catholytes for Effective Macromolecular Separation in Nonaqueous Redox Flow Batteries. *ACS Cent. Sci.* **2018**, *4*, 189−196.
(31) Doris, S. E.; Ward, A. L.; Baskin, A.; Frischmann, P. D.; Gavvalapalli, N.; Chénard, E.; Sevov, C. S.; Prendergast, D.; Moore, J. S.; Helms, B. A. Macromolecular Design Strategies for Preventing Active-Material Crossover in Non-Aqueous All-Organic Redox-Flow Batteries. *Angew. Chem., Int. Ed.* **2017**, *56*, 1595−1599.
(32) Goulet, M. A.; Tong, L.; Pollack, D. A.; Tabor, D. P.; Odom, S. A.; Aspuru-Guzik, A.; Kwan, E. E.; Gordon, R. G.; Aziz, M. J. Extending the Lifetime of Organic Flow Batteries via Redox State Management. *J. Am. Chem. Soc.* **2019**, *141*, 8014−8019.
(33) Goulet, M.-A.; Aziz, M. J. Flow Battery Molecular Reactant Stability Determined by Symmetric Cell Cycling Methods. *J. Electrochem. Soc.* **2018**, *165*, A1466−A1477.
(34) Hollas, A.; Wei, X.; Murugesan, V.; Nie, Z.; Li, B.; Reed, D.; Liu, J.; Sprenkle, V.; Wang, W. A biomimetic high-capacity phenazine-based anolyte for aqueous organic redox flow batteries. *Nat. Energy* **2018**, *3*, 508−514.
(35) Sun, P.; Liu, Y.; Li, Y.; Shehzad, M. A.; Liu, Y.; Zuo, P.; Chen, Q.; Yang, Z.; Xu, T. 110th Anniversary: Unleashing the Full Potential of Quinones for High Performance Aqueous Organic Flow Battery. *Ind. Eng. Chem. Res.* **2019**, *58*, 3994−3999.
(36) Yang, Z. J.; Tong, L. C.; Tabor, D. P.; Beh, E. S.; Goulet, M. A.; De Porcellinis, D.; Aspuru-Guzik, A.; Gordon, R. G.; Aziz, M. J. Alkaline Benzoquinone Aqueous Flow Battery for Large-Scale Storage of Electrical Energy. *Adv. Energy Mater.* **2018**, *8*, 1702056.
(37) Darling, R.; Gallagher, K.; Xie, W.; Su, L.; Brushett, F. Transport Property Requirements for Flow Battery Separators. *J. Electrochem. Soc.* **2016**, *163*, A5029−A5040.
(38) Darling, R. M.; Weber, A. Z.; Tucker, M. C.; Perry, M. L. The Influence of Electric Field on Crossover in Redox-Flow Batteries. *J. Electrochem. Soc.* **2016**, *163*, A5014−A5022.
(39) Ashraf Gandomi, Y.; Aaron, D. S.; Mench, M. M. Coupled Membrane Transport Parameters for Ionic Species in All-Vanadium Redox Flow Batteries. *Electrochim. Acta* **2016**, *218*, 174−190.
(40) Luo, Q.; Li, L.; Nie, Z.; Wang, W.; Wei, X.; Li, B.; Chen, B.; Yang, Z. *In-situ* investigation of vanadium ion transport in redox flow battery. *J. Power Sources* **2012**, *218*, 15−20.
(41) Chen, H.; Cong, G.; Lu, Y.-C. Recent progress in organic redox flow batteries: Active materials, electrolytes and membranes. *J. Energy Chem.* **2018**, *27*, 1304−1325.
(42) Wei, X. L.; Pan, W. X.; Duan, W. T.; Hollas, A.; Yang, Z.; Li, B.; Nie, Z. M.; Liu, J.; Reed, D.; Wang, W.; Sprenkle, V. Materials and Systems for Organic Redox Flow Batteries: Status and Challenges. *ACS Energy Lett.* **2017**, *2*, 2187−2204.
(43) Leung, P.; Shah, A. A.; Sanz, L.; Flox, C.; Morante, J. R.; Xu, Q.; Mohamed, M. R.; Ponce de León, C.; Walsh, F. C. Recent developments in organic redox flow batteries: A critical review. *J. Power Sources* **2017**, *360*, 243−283.
(44) Leung, P.; Li, X.; Ponce de León, C.; Berlouis, L.; Low, C. T. J.; Walsh, F. C. Progress in redox flow batteries, remaining challenges and their applications in energy storage. *RSC Adv.* **2012**, *2*, 10125.
(45) Chen, R. Toward High-Voltage, Energy-Dense, and Durable Aqueous Organic Redox Flow Batteries: Role of the Supporting Electrolytes. *ChemElectroChem* **2019**, *6*, 603−612.
(46) Singh, V.; Kim, S.; Kang, J.; Byon, H. R. Aqueous organic redox flow batteries. *Nano Res.* **2019**, *12*, 1988−2001.
(47) Luo, J. A.; Hu, B.; Hu, M. W.; Zhao, Y.; Liu, T. L. Status and Prospects of Organic Redox Flow Batteries toward Sustainable Energy Storage. *ACS Energy Lett.* **2019**, *4*, 2220−2240.
(48) Er, S.; Suh, C.; Marshak, M. P.; Aspuru-Guzik, A. Computational Design of Molecules for an All-Quinone Redox Flow Battery. *Chem. Sci.* **2015**, *6*, 885−893.
(49) Huynh, M. T.; Anson, C. W.; Cavell, A. C.; Stahl, S. S.; Hammes-Schiffer, S. Quinone 1 e- and 2 e-/2 H+ Reduction Potentials: Identification and Analysis of Deviations from Systematic Scaling Relationships. *J. Am. Chem. Soc.* **2016**, *138*, 15903−15910.
(50) Kim, H.; Goodson, T.; Zimmerman, P. M. Achieving Accurate Reduction Potential Predictions for Anthraquinones in Water and Aprotic Solvents: Effects of Inter- and Intramolecular H-Bonding and Ion Pairing. *J. Phys. Chem. C* **2016**, *120*, 22235−22247.
(51) Lim, H.-D.; Lee, B.; Zheng, Y.; Hong, J.; Kim, J.; Gwon, H.; Ko, Y.; Lee, M.; Cho, K.; Kang, K. Rational design of redox mediators for advanced Li-O2 batteries. *Nat. Energy* **2016**, *1*, 16066.
(52) Gerhardt, M. R.; Tong, L. C.; Gomez-Bombarelli, R.; Chen, Q.; Marshak, M. P.; Galvin, C. J.; Aspuru-Guzik, A.; Gordon, R. G.; Aziz, M. J. Anthraquinone Derivatives in Aqueous Flow Batteries. *Adv. Energy Mater.* **2017**, *7*, 1601488.
(53) Kwabi, D. G.; Lin, K.; Ji, Y.; Kerr, E. F.; Goulet, M.-A.; De Porcellinis, D.; Tabor, D. P.; Pollack, D. A.; Aspuru-Guzik, A.; Gordon, R. G.; Aziz, M. J. Alkaline quinone flow battery with long lifetime at pH 12. *Joule* **2018**, *2*, 1907.
(54) Ji, Y.; Goulet, M.-A.; Pollack, D. A.; Kwabi, D. G.; Jin, S.; Porcellinis, D.; Kerr, E. F.; Gordon, R. G.; Aziz, M. J. A Phosphonate-Functionalized Quinone Redox Flow Battery at Near-Neutral pH with Record Capacity Retention Rate. *Adv. Energy Mater.* **2019**, *9*, 1900039.
(55) Han, K. S.; Rajput, N. N.; Vijayakumar, M.; Wei, X.; Wang, W.; Hu, J.; Persson, K. A.; Mueller, K. T. Preferential Solvation of an Asymmetric Redox Molecule. *J. Phys. Chem. C* **2016**, *120*, 27834−27839.
(56) Luo, J.; Hu, B.; Debruler, C.; Bi, Y.; Zhao, Y.; Yuan, B.; Hu, M.; Wu, W.; Liu, T. L. Unprecedented capacity and stability of ammonium ferrocyanide catholyte in pH neutral aqueous redox flow batteries. *Joule* **2019**, *3*, 149−163.
(57) Hamlin, T. A.; Swart, M.; Bickelhaupt, F. M. Nucleophilic Substitution (SN2): Dependence on Nucleophile, Leaving Group, Central Atom, Substituents, and Solvent. *ChemPhysChem* **2018**, *19*, 1315−1330.
(58) Smith, M. B.; March, J. *March's Advanced Organic Chemistry: Reactions, Mechanisms, and Structure*, 6th ed.; Wiley: Hoboken, NJ, 2007.
(59) Tabor, D. P.; Gómez-Bombarelli, R.; Tong, L.; Gordon, R. G.; Aziz, M. J.; Aspuru-Guzik, A. Mapping the frontiers of quinone stability in aqueous media: implications for organic aqueous redox flow batteries. *J. Mater. Chem. A* **2019**, *7*, 12833−12841.
(60) Huskinson, B.; Marshak, M. P.; Suh, C.; Er, S.; Gerhardt, M. R.; Galvin, C. J.; Chen, X.; Aspuru-Guzik, A.; Gordon, R. G.; Aziz, M. J. A metal-free organic-inorganic aqueous flow battery. *Nature* **2014**, *505*, 195−198.
(61) Murali, A.; Nirmalchandar, A.; Krishnamoorthy, S.; Hoober-Burkhardt, L.; Yang, B.; Soloveichik, G.; Prakash, G. K. S.; Narayanan, S. R. Understanding and mitigating capacity fade in aqueous organic redox flow batteries. *J. Electrochem. Soc.* **2018**, *165*, A1193.
(62) Liu, T.; Wei, X.; Nie, Z.; Sprenkle, V.; Wang, W. A Total Organic Aqueous Redox Flow Battery Employing a Low Cost and Sustainable Methyl Viologen Anolyte and 4-HO-TEMPO Catholyte. *Adv. Energy Mater.* **2016**, *6*, 1501449.
(63) Orita, A.; Verde, M. G.; Sakai, M.; Meng, Y. S. The impact of pH on side reactions for aqueous redox flow batteries based on nitroxyl radical compounds. *J. Power Sources* **2016**, *321*, 126−134.
(64) Luo, J.; Sam, A.; Hu, B.; DeBruler, C.; Wei, X.; Wang, W.; Liu, T. L. Unraveling pH Dependent Cycling Stability of Ferricyanide/Ferrocyanide in Redox Flow Batteries. *Nano Energy* **2017**, *42*, 215−221.
(65) Kumpan, N.; Poonsawat, T.; Chaicharoenwimolkul, L.; Pornsuwan, S.; Somsook, E. Ferrocenated nanocatalysts derived from the decomposition of ferrocenium in basic solution and their aerobic activities for the rapid decolorization of methylene blue and the facile oxidation of phenylboronic acid. *RSC Adv.* **2017**, *7*, 5759−5763.
(66) Tabbì, G.; Cassino, C.; Cavigiolio, G.; Colangelo, D.; Ghiglia, A.; Viano, I.; Osella, D. Water Stability and Cytotoxic Activity Relationship of a Series of Ferrocenium Derivatives. ESR Insights on the Radical Production during the Degradation Process. *J. Med. Chem.* **2002**, *45*, 5786−5796.
(67) Thomas, J.-L.; Howarth, J.; Hanlon, K.; McGuirk, D. Ferrocenyl imidazolium salts as a new class of anion receptors with C-H&X-hydrogen bonding. *Tetrahedron Lett.* **2000**, *41*, 413−416.

https://dx.doi.org/10.1021/acs.chemrev.9b00599
Chem. Rev. 2020, 120, 6467−6489

(68) Gasser, G.; Fischmann, A. J.; Forsyth, C. M.; Spiccia, L. Products of hydrolysis of (ferrocenylmethyl)trimethylammonium iodide: Synthesis of hydroxymethylferrocene and bis(ferrocenylmethyl) ether. *J. Organomet. Chem.* **2007**, *692*, 3835−3840.
(69) Bird, C. L.; Kuhn, A. T. Electrochemistry of the viologens. *Chem. Soc. Rev.* **1981**, *10*, 49−82.
(70) Murugavel, K. Benzylic viologen dendrimers: a review of their synthesis, properties and applications. *Polym. Chem.* **2014**, *5*, 5873−5884.
(71) Bard, A. J.; Ledwith, A.; Shine, H. J. Formation, Properties and Reactions of Cation Radicals in Solution. *Adv. Phys. Org. Chem.* **1976**, *13*, 155−278.
(72) Venturi, M.; Mulazzani, Q. G.; Hoffman, M. Z. Radiolytically-induced one-electron reduction of methyl viologen in aqueous solution. *Radiat. Phys. Chem.* **1984**, *23*, 229−236.
(73) O'Connor, C. Acidic and basic amide hydrolysis. *Q. Rev., Chem. Soc.* **1970**, *24*, 553−564.
(74) Koziol, J.; Tyrakowska, B.; Muller, F. The Structure of Covalent Hydrates) of Alloxazines - a Reinvestigation. *Helv. Chim. Acta* **1981**, *64*, 1812−1817.
(75) Koziol, J.; Metzler, D. E. Formation and Possible Structure of Covalent Hydrates of Alloxazines. *Z. Naturforsch., B: J. Chem. Sci.* **1972**, *27*, 1027−1029.
(76) Smith, S. B.; Bruice, T. C. Mechanisms of isoalloxazine (flavine) hydrolysis. *J. Am. Chem. Soc.* **1975**, *97*, 2875−2881.
(77) Surrey, A. R.; Nachod, F. C. Alkaline Hydrolysis of Riboflavin. *J. Am. Chem. Soc.* **1951**, *73*, 2336−2338.
(78) Harayama, T.; Tezuka, Y.; Taga, T.; Yoneda, F. Hydrolysis Products of Flavins (Isoalloxazines). *J. Chem. Soc., Perkin Trans. 1* **1987**, 75−83.
(79) Lin, K.; Gómez-Bombarelli, R.; Beh, E. S.; Tong, L.; Chen, Q.; Valle, A.; Aspuru-Guzik, A.; Aziz, M. J.; Gordon, R. G. A redox-flow battery with an alloxazine-based organic electrolyte. *Nat. Energy* **2016**, *1*, 16102.
(80) Beck, F.; Heydecke, G. On the Mechanism of the Cathodic Reduction of Anthraquinone to Anthrone. *Ber. Bunsenges. Phys. Chem.* **1987**, *91*, 37−43.
(81) Shi, Z.-W.; Li, Y.-Z.; Li, Y.; Lu, G.-Y.; Liu, S.-H. 1,1′,8,8′-Tetramethoxy-10,10′-bianthrone. *Acta Crystallogr., Sect. E: Struct. Rep. Online* **2004**, *60*, No. o2275.
(82) Jin, S.; Jing, Y.; Kwabi, D. G.; Ji, Y.; Tong, L.; De Porcellinis, D.; Goulet, M.-A.; Pollack, D. A.; Gordon, R. G.; Aziz, M. J. A Water-Miscible Quinone Flow Battery with High Volumetric Capacity and Energy Density. *ACS Energy Lett.* **2019**, *4*, 1342−1348.
(83) Antonov, L. *Tautomerism: Methods and Theories*; Wiley-VCH: Weinheim, Germany, 2013.
(84) Deuchert, K.; Hünig, S. Multistage Organic Redox Systems—A General Structural Principle. *Angew. Chem., Int. Ed. Engl.* **1978**, *17*, 875−886.
(85) Thomson, R. H. Phenol tautomerism. *Q. Rev., Chem. Soc.* **1956**, *10*, 27−43.
(86) Thomson, R. H. 352. The structure of β-hydrojuglone and related compounds. Keto-;enols of the naphthalene series. *J. Chem. Soc.* **1950**, *0*, 1737−1742.
(87) Saveant, J.-M. *Elements of Molecular and Biomolecular Electrochemistry*; Wiley: Hoboken, NJ, 2006.
(88) Chen, Q.; Eisenach, L.; Aziz, M. J. Cycling Analysis of a Quinone-Bromide Redox Flow Battery. *J. Electrochem. Soc.* **2016**, *163*, A5057−A5063.
(89) Chen, Q.; Gerhardt, M. R.; Aziz, M. J. Dissection of the voltage losses of an acidic quinone redox flow battery. *J. Electrochem. Soc.* **2017**, *164*, A1126−A1132.
(90) Beh, E. S.; De Porcellinis, D.; Gracia, R. L.; Xia, K. T.; Gordon, R. G.; Aziz, M. J. A neutral pH aqueous organic-organometallic redox flow battery with extremely high capacity retention. *ACS Energy Lett.* **2017**, *2*, 639−644.
(91) Xu, Y.; Wen, Y. H.; Cheng, J.; Cao, G. P.; Yang, Y. S. A study of tiron in aqueous solutions for redox flow battery application. *Electrochim. Acta* **2010**, *55*, 715−720.
(92) Xu, Y.; Wen, Y.; Cheng, J.; Cao, G.; Yang, Y. Study on a single flow acid Cd-chloranil battery. *Electrochem. Commun.* **2009**, *11*, 1422−1424.
(93) Nawar, S.; Huskinson, B.; Aziz, M. Benzoquinone-Hydroquinone Couple for Flow Battery. *MRS Proceedings* **2013**, *1491*, 1491.
(94) Huskinson, B.; Nawar, S.; Gerhardt, M. R.; Aziz, M. J. Novel Quinone-Based Couples for Flow Batteries. *ECS Trans.* **2013**, *53*, 101−105.
(95) Yang, B.; Hoober-Burkhardt, L.; Krishnamoorthy, S.; Murali, A.; Prakash, G. K. S.; Narayanan, S. R. High-Performance Aqueous Organic Flow Battery with Quinone-Based Redox Couples at Both Electrodes. *J. Electrochem. Soc.* **2016**, *163*, A1442−A1449.
(96) Hoober-Burkhardt, L.; Krishnamoorthy, S.; Yang, B.; Murali, A.; Nirmalchandar, A.; Prakash, G. K. S.; Narayanan, S. R. A new Michael-reaction-resistant benzoquinone for aqueous organic redox flow batteries. *J. Electrochem. Soc.* **2017**, *164*, A600−A607.
(97) Yang, B.; Prakash, G. K. S.; Aniszfeld, R.; Narayan, S. R.; Hoober-Burkhardt, L.; Krishnamoorthy, S.; Murali, A.; Nirmalchandar, A. Stable Positive Side Material for All-Organic Flow Battery. U.S. Patent Application 2019/0115594 A1, 2019.
(98) Tong, L.; Goulet, M.-A.; Tabor, D. P.; Kerr, E. F.; De Porcellinis, D.; Fell, E. M.; Aspuru-Guzik, A.; Gordon, R. G.; Aziz, M. J. Molecular Engineering of an Alkaline Naphthoquinone Flow Battery. *ACS Energy Lett.* **2019**, *4*, 1880−1887.
(99) Jin, S.; Jing, Y.; Kwabi, D. G.; Ji, Y.; Tong, L.; De Porcellinis, D.; Goulet, M.-A.; Pollack, D. A.; Gordon, R. G.; Aziz, M. J. A Water-Miscible Quinone Flow Battery with High Volumetric Capacity and Energy Density. *ACS Energy Letters* **2019**, *4*, 1342−1348.
(100) Wang, C.; Yang, Z.; Wang, Y.; Zhao, P.; Yan, W.; Zhu, G.; Ma, L.; Yu, B.; Wang, L.; Li, G.; Liu, J.; Jin, Z. High-performance alkaline organic redox flow batteries based on 2-hydroxy-3-carboxy-1,4-naphthoquinone. *ACS Energy Lett.* **2018**, *3*, 2404−2409.
(101) Yang, B.; Hoober-Burkhardt, L.; Wang, F.; Surya Prakash, G. K.; Narayanan, S. R. An inexpensive aqueous flow battery for large-scale electrical energy storage based on water-soluble organic redox couples. *J. Electrochem. Soc.* **2014**, *161*, A1371−A1380.
(102) Zhang, S.; Li, X.; Chu, D. An Organic Electroactive Material for Flow Batteries. *Electrochim. Acta* **2016**, *190*, 737−743.
(103) Park, M.; Beh, E. S.; Fell, E. M.; Jing, Y.; Kerr, E. F.; Porcellinis, D.; Goulet, M.-A.; Ryu, J.; Wong, A. A.; Gordon, R. G.; Cho, J.; Aziz, M. J. A high voltage aqueous zinc-organic hybrid flow battery. *Adv. Energy Mater.* **2019**, *9*, 1900694.
(104) Wedege, K.; Dražević, E.; Konya, D.; Bentien, A. Organic Redox Species in Aqueous Flow Batteries: Redox Potentials, Chemical Stability and Solubility. *Sci. Rep.* **2016**, *6*, 39101.
(105) Leung, P. K.; Martin, T.; Shah, A. A.; Anderson, M. A.; Palma, J. Membrane-less organic-inorganic aqueous flow batteries with improved cell potential. *Chem. Commun.* **2016**, *52*, 14270−14273.
(106) Xu, Y.; Zheng, Y.; Wang, C.; Chen, Q. An All-Organic Aqueous Battery Powered by Adsorbed Quinone. *ACS Appl. Mater. Interfaces* **2019**, *11*, 23222−23228.
(107) Preger, Y.; Gerken, J. B.; Biswas, S.; Anson, C. W.; Johnson, M. R.; Root, T. W.; Stahl, S. S. Quinone-Mediated Electrochemical O2 Reduction Accessing High Power Density with an Off-Electrode Co-N/C Catalyst. *Joule* **2018**, *2*, 2722−2731.
(108) Carney, T. J.; Collins, S. J.; Moore, J. S.; Brushett, F. R. Concentration-Dependent Dimerization of Anthraquinone Disulfonic Acid and Its Impact on Charge Storage. *Chem. Mater.* **2017**, *29*, 4801−4810.
(109) Wiberg, C.; Carney, T. J.; Brushett, F.; Ahlberg, E.; Wang, E. Dimerization of 9,10-anthraquinone-2,7-Disulfonic acid (AQDS). *Electrochim. Acta* **2019**, *317*, 478−485.
(110) Gerhardt, M. R.; Beh, E. S.; Tong, L.; Gordon, R. G.; Aziz, M. J. Comparison of Capacity Retention Rates During Cycling of Quinone-Bromide Flow Batteries. *MRS Adv.* **2017**, *2*, 431−438.
(111) Wedege, K.; Azevedo, J.; Khataee, A.; Bentien, A.; Mendes, A. Direct Solar Charging of an Organic-Inorganic, Stable, and Aqueous Alkaline Redox Flow Battery with a Hematite Photoanode. *Angew. Chem., Int. Ed.* **2016**, *55*, 7142−7147.

https://dx.doi.org/10.1021/acs.chemrev.9b00599
Chem. Rev. 2020, 120, 6467−6489

(112) Li, W.; Fu, H. C.; Li, L.; Caban-Acevedo, M.; He, J. H.; Jin, S. Integrated Photoelectrochemical Solar Energy Conversion and Organic Redox Flow Battery Devices. *Angew. Chem., Int. Ed.* **2016**, *55*, 13104−13108.
(113) McKone, J. R.; DiSalvo, F. J.; Abruna, H. D. Solar energy conversion, storage, and release using an integrated solar-driven redox flow battery. *J. Mater. Chem. A* **2017**, *5*, 5362−5372.
(114) Kwabi, D. G.; Wong, A. A.; Aziz, M. J. Rational Evaluation and Cycle Life Improvement of Quinone-Based Aqueous Flow Batteries Guided by In-Line Optical Spectrophotometry. *J. Electrochem. Soc.* **2018**, *165*, A1770−A1776.
(115) Xie, W.; Darling, R. M.; Perry, M. L. Processing and Pretreatment Effects on Vanadium Transport in Nafion Membranes. *J. Electrochem. Soc.* **2016**, *163*, A5084−A5089.
(116) Smith, M. B. *March's Advanced Organic Chemistry: Reactions, Mechanisms, and Structure*, 5th ed.; Wiley-VCH: Weinheim, Germany, 2001.
(117) Chang, Z.; Henkensmeier, D.; Chen, R. One-Step Cationic Grafting of 4-Hydroxy-TEMPO and its Application in a Hybrid Redox Flow Battery with a Crosslinked PBI Membrane. *ChemSusChem* **2017**, *10*, 3193−3197.
(118) Liu, Y.; Goulet, M.-A.; Tong, L.; Liu, Y.; Ji, Y.; Wu, L.; Gordon, R. G.; Aziz, M. J.; Yang, Z.; Xu, T. A Long-Lifetime All-Organic Aqueous Flow Battery Utilizing TMAP-TEMPO Radical. *Chem.* **2019**, *5*, 1861−1870.
(119) Winsberg, J.; Stolze, C.; Muench, S.; Liedl, F.; Hager, M. D.; Schubert, U. S. TEMPO/phenazine combi-molecule: a redox-active material for symmetric aqueous redox-flow batteries. *ACS Energy Lett.* **2016**, *1*, 976−980.
(120) Janoschka, T.; Martin, N.; Martin, U.; Friebe, C.; Morgenstern, S.; Hiller, H.; Hager, M. D.; Schubert, U. S. An aqueous, polymer-based redox-flow battery using non-corrosive, safe, and low-cost materials. *Nature* **2015**, *527*, 78−81.
(121) Janoschka, T.; Martin, N.; Hager, M. D.; Schubert, U. S. An aqueous redox-flow battery with high capacity and power: the TEMPTMA/MV system. *Angew. Chem., Int. Ed.* **2016**, *55*, 14427−14430.
(122) Luo, J.; Hu, B.; DeBruler, C.; Liu, T. A "π-Conjugation Extended Viologen" as Novel Two-Electron Storage Anolyte for Total Organic Aqueous Redox Flow Battery. *Angew. Chem., Int. Ed.* **2018**, *57*, 231−235.
(123) Chang, Z.; Henkensmeier, D.; Chen, R. Shifting redox potential of nitroxyl radical by introducing an imidazolium substituent and its use in aqueous flow batteries. *J. Power Sources* **2019**, *418*, 11−16.
(124) Winsberg, J.; Stolze, C.; Schwenke, A.; Muench, S.; Hager, M. D.; Schubert, U. S. Aqueous 2,2,6,6-Tetramethylpiperidine-N-oxyl Catholytes for a High-Capacity and High Current Density Oxygen-Insensitive Hybrid-Flow Battery. *ACS Energy Lett.* **2017**, *2*, 411−416.
(125) Hu, B.; DeBruler, C.; Rhodes, Z.; Liu, T. L. Long-cycling aqueous organic redox flow battery (AORFB) toward sustainable and safe energy storage. *J. Am. Chem. Soc.* **2017**, *139*, 1207−1214.
(126) Gong, K.; Xu, F.; Grunewald, J. B.; Ma, X.; Zhao, Y.; Gu, S.; Yan, Y. All-Soluble All-Iron Aqueous Redox-Flow Battery. *ACS Energy Lett.* **2016**, *1*, 89−93.
(127) DeBruler, C.; Hu, B.; Moss, J.; Luo, J.; Liu, T. L. A sulfonate-functionalized viologen enabling neutral cation exchange, aqueous organic redox flow batteries toward renewable energy storage. *ACS Energy Lett.* **2018**, *3*, 663−668.
(128) Huang, J. H.; Yang, Z.; Murugesan, V.; Walter, E.; Hollas, A.; Pan, B. F.; Assary, R. S.; Shkrob, I. A.; Wei, X. L.; Zhang, Z. C. Spatially Constrained Organic Diquat Anolyte for Stable Aqueous Flow Batteries. *ACS Energy Lett.* **2018**, *3*, 2533−2538.
(129) DeBruler, C.; Hu, B.; Moss, J.; Liu, X. A.; Luo, J. A.; Sun, Y. J.; Liu, T. L. Designer Two-Electron Storage Viologen Anolyte Materials for Neutral Aqueous Organic Redox Flow Batteries. *Chem.* **2017**, *3*, 961−978.
(130) Hu, B.; Tang, Y.; Luo, J.; Grove, G.; Guo, Y.; Liu, T. Improved Radical Stability of Viologen Anolyte in Aqueous Organic Redox Flow Battery. *Chem. Commun.* **2018**, *54*, 6871−6874.
(131) Varcoe, J. R.; Atanassov, P.; Dekel, D. R.; Herring, A. M.; Hickner, M. A.; Kohl, P. A.; Kucernak, A. R.; Mustain, W. E.; Nijmeijer, K.; Scott, K.; Xu, T.; Zhuang, L. Anion-exchange membranes in electrochemical energy systems. *Energy Environ. Sci.* **2014**, *7*, 3135−3191.
(132) Zhu, Y.; Yang, F.; Niu, Z.; Wu, H.; He, Y.; Zhu, H.; Ye, J.; Zhao, Y.; Zhang, X. Enhanced cyclability of organic redox flow batteries enabled by an artificial bipolar molecule in neutral aqueous electrolyte. *J. Power Sources* **2019**, *417*, 83−89.
(133) Yu, X. W.; Manthiram, A. A strategically managed rechargeable battery system with a neutral methyl viologen anolyte and an acidic air-cathode enabled by a mediator-ion solid electrolyte. *Sustainable Energy & Fuels* **2018**, *2*, 1452−1457.
(134) Winsberg, J.; Hagemann, T.; Muench, S.; Friebe, C.; Häupler, B.; Janoschka, T.; Morgenstern, S.; Hager, M. D.; Schubert, U. S. Poly(boron-dipyrromethene)—A Redox-Active Polymer Class for Polymer Redox-Flow Batteries. *Chem. Mater.* **2016**, *28*, 3401−3405.
(135) Winsberg, J.; Janoschka, T.; Morgenstern, S.; Hagemann, T.; Muench, S.; Hauffman, G.; Gohy, J. F.; Hager, M. D.; Schubert, U. S. Poly(TEMPO)/Zinc Hybrid-Flow Battery: A Novel, "Green," High Voltage, and Safe Energy Storage System. *Adv. Mater.* **2016**, *28*, 2238−2243.
(136) Winsberg, J.; Muench, S.; Hagemann, T.; Morgenstern, S.; Janoschka, T.; Billing, M.; Schacher, F. H.; Hauffman, G.; Gohy, J.-F.; Hoeppener, S.; Hager, M. D.; Schubert, U. S. Polymer/zinc hybrid-flow battery using block copolymer micelles featuring a TEMPO corona as catholyte. *Polym. Chem.* **2016**, *7*, 1711−1718.
(137) Häupler, B.; Rössel, C.; Schwenke, A. M.; Winsberg, J.; Schmidt, D.; Wild, A.; Schubert, U. S. Aqueous zinc-organic polymer battery with a high rate performance and long lifetime. *NPG Asia Mater.* **2016**, *8*, No. e283.
(138) Milshtein, J. D.; Su, L.; Liou, C.; Badel, A. F.; Brushett, F. R. Voltammetry study of quinoxaline in aqueous electrolytes. *Electrochim. Acta* **2015**, *180*, 695−704.
(139) Orita, A.; Verde, M. G.; Sakai, M.; Meng, Y. S. A biomimetic redox flow battery based on flavin mononucleotide. *Nat. Commun.* **2016**, *7*, 13230.
(140) Sevov, C. S.; Hendriks, K. H.; Sanford, M. S. Low-Potential Pyridinium Anolyte for Aqueous Redox Flow Batteries. *J. Phys. Chem. C* **2017**, *121*, 24376−24380.
(141) Huang, Z. F.; Zhang, P.; Gao, X. P.; Henkensmeier, D.; Passerini, S.; Chen, R. Y. Unlocking Simultaneously the Temperature and Electrochemical Windows of Aqueous Phthalocyanine Electrolytes. *Acs Applied Energy Materials* **2019**, *2*, 3773−3779.
(142) Leung, P.; Aili, D.; Xu, Q.; Rodchanarowan, A.; Shah, A. A. Rechargeable organic-air redox flow batteries. *Sustain. Energy Fuels* **2018**, *2*, 2252−2259.
(143) Hong, J.; Kim, K. Neutral Red and Ferroin as Reversible and Rapid Redox Materials for Redox Flow Batteries. *ChemSusChem* **2018**, *11*, 1866−1872.
(144) Brushett, F.; Jansen, A. N.; Vaughey, J. T.; Su, L.; Milshtein, J. D. Materials for use with aqueous redox flow batteries and related methods and systems. U.S. Patent 14,625,417, 2015.
(145) Zhang, C.; Niu, Z.; Peng, S.; Ding, Y.; Zhang, L.; Guo, X.; Zhao, Y.; Yu, G. Phenothiazine-Based Organic Catholyte for High-Capacity and Long-Life Aqueous Redox Flow Batteries. *Adv. Mater.* **2019**, *31*, 1901052.
(146) McCormick, D. B.; Fory, W. Base-Catalyzed Hydrolysis of Flavins - Effect of Amines and Particular Role of Position 3. *J. Pharm. Sci.* **1968**, *57*, 841−844.
(147) Grajek, H.; Zurkowska, G.; Drabent, R.; Bojarski, C. The structure of the flavomononucleotide dimer. *Biochim. Biophys. Acta, Gen. Subj.* **1986**, *881*, 241−247.
(148) Darling, R. M.; Perry, M. L. Half-Cell, Steady-State Flow-Battery Experiments. *ECS Trans.* **2013**, *53*, 31−38.
(149) Milshtein, J. D.; Barton, J. L.; Darling, R. M.; Brushett, F. R. 4-acetamido-2,2,6,6-tetramethylpiperidine-1-oxyl as a model organic redox active compound for nonaqueous flow batteries. *J. Power Sources* **2016**, *327*, 151−159.

https://dx.doi.org/10.1021/acs.chemrev.9b00599
Chem. Rev. 2020, 120, 6467−6489

(150) Milshtein, J. D.; Kaur, A. P.; Casselman, M. D.; Kowalski, J. A.; Modekrutti, S.; Zhang, P. L.; Harsha Attanayake, N.; Elliott, C. F.; Parkin, S. R.; Risko, C.; Brushett, F. R.; Odom, S. A. High current density, long duration cycling of soluble organic active species for non-aqueous redox flow batteries. *Energy Environ. Sci.* **2016**, *9*, 3531−3543.
(151) Drazevic, E.; Szabo, C.; Konya, D.; Lund, T.; Wedege, K.; Bentien, A. Investigation of Tetramorpholinohydroquinone as a Potential Catholyte in a Flow Battery. *ACS Appl. Energy Mater.* **2019**, *2*, 4745−4754.
(152) Hu, B.; Luo, J.; Hu, M.; Yuan, B.; Liu, T. L. A pH-Neutral, Metal-Free Aqueous Organic Redox Flow Battery Employing an Ammonium Anthraquinone Anolyte. *Angew. Chem., Int. Ed.* **2019**, *58*, 16629−16636.
(153) Huskinson, B.; Marshak, M. P.; Gerhardt, M. R.; Aziz, M. J. Cycling of a Quinone-Bromide Flow Battery for Large-Scale Electrochemical Energy Storage. *ECS Trans.* **2014**, *61*, 27−30.
(154) Asperger, S. Kinetics of the decomposition of potassium ferrocyanide in ultra-violet light. *Trans. Faraday Soc.* **1952**, *48*, 617−624.
(155) Arellano, C. A. P.; Martínez, S. S. Effects of pH on the degradation of aqueous ferricyanide by photolysis and photocatalysis under solar radiation. *Sol. Energy Mater. Sol. Cells* **2010**, *94*, 327−332.
(156) Esswein, A. J.; Goeltz, J.; Amadeo, D. High Solubility Iron Hexacyanides. U.S. Patent 13,887,461, 2014.

https://dx.doi.org/10.1021/acs.chemrev.9b00599
Chem. Rev. 2020, 120, 6467−6489